

This work was written as part of one of the author's official duties as an Employee of the United States Government and is therefore a work of the United States Government. In accordance with 17 U.S.C. 105, no copyright protection is available for such works under U.S. Law.

Public Domain Mark 1.0

<https://creativecommons.org/publicdomain/mark/1.0/>

Access to this work was provided by the University of Maryland, Baltimore County (UMBC) ScholarWorks@UMBC digital repository on the Maryland Shared Open Access (MD-SOAR) platform.

Please provide feedback

Please support the ScholarWorks@UMBC repository by emailing scholarworks-group@umbc.edu and telling us what having access to this work means to you and why it's important to you. Thank you.

Nimbus-7 Global Cloud Climatology. Part II: First Year Results

LARRY L. STOWE

NOAA/NESDIS, Washington, D.C.

H. Y. MICHAEL YEH*

ST Systems Corporation, Hyattsville, Maryland

THOMAS F. ECK

Science Application Research, Lanham, Maryland

CHARLIE G. WELLEMAYER

ST Systems Corporation, Hyattsville, Maryland

H. LEE KYLE

NASA/Goddard Space Flight Center, Greenbelt, Maryland

THE NIMBUS-7 CLOUD DATA PROCESSING TEAM[†]

(Manuscript received 6 May 1988, in final form 30 November 1988)

ABSTRACT

Regional and seasonal variations in global cloud cover observed by the Nimbus-7 satellite over 1 year are analyzed by examining the 4 midseason months—April, July and October 1979 and January 1980. The Nimbus-7 data set is generated from the Temperature Humidity Infrared Radiometer (THIR) 11.5 micron radiances together with Total Ozone Mapping Spectrometer (TOMS)-derived UV reflectivities, climatological atmospheric temperature lapse rates, and concurrent surface temperature and snow/ice information from the Air Force three-dimensional-nephelometer (3DN) archive. The analysis presented here includes total cloud amount, cloud amounts at high, middle and low altitudes, cirrus and deep convective clouds and cloud and clear-sky 11.5 micron-derived radiances. Also, noon versus midnight cloud amounts are examined and the Nimbus-7 data are compared to three previously published cloud climatologies.

The Nimbus-7 bispectral algorithm gives a monthly mean global noontime cloud cover of 51%, averaged over the 4 months. When only the IR is used, this cloud cover is 49% at noontime and 56% at midnight, indicating that the Earth's cloud cover has a substantial diurnal cycle. Each hemisphere shows a cloud cover maximum in its summer and a minimum in its winter. The Southern Hemisphere shows more clouds than the Northern Hemisphere except for the month of July.

The difference between the cloud-top and clear-scene radiance has maxima in the equatorial cloud belt and minima in the polar regions. Because of these polar minima and the frequent presence of snow, Nimbus-7 cloud fraction estimates are less reliable in the polar regions. In the tropics the data show more clouds at midnight than at noon. Over the tropical ocean, overcast regions show lower cloud top radiation temperatures at noon than at midnight, but over land the reverse occurs.

In July, cloud amounts in the intertropical convergence zone (ITCZ) peak at about 10°N latitude with local maxima greater than 70% around the west coasts of Africa and Central America, and from India east to the dateline. Cloud-top radiances indicate that mid- and high-level clouds predominate in the ITCZ, with 5% to 15% each of cirrus and deep convective clouds, respectively. In January, the peak of the ITCZ shifts to 10°S with local cloud maxima greater than 90% over Brazil and to the north and northwest of Australia. Comparison is made with several other cloud data sets, including a look at the new preliminary International Satellite Cloud Climatology Project (ISCCP) results. There are considerable differences among the several data sets examined.

* Present affiliation: Caelum Research Corporation, Silver Spring, Maryland.

[†] The Nimbus-7 Cloud Data Processing Team Members: H. L. Kyle, Team Manager, P. H. Hwang, Former Team Manager, NASA/GSFC; L. L. Stowe, Principal Scientist, P. P. Pellegrino, NOAA/NESDIS; P. K. Bhartia, H. D. Chang, C. S. Long, C. G. Wellemeyer,

and H. Y. M. Yeh, ST Systems Corporation; T. F. Eck, Science Applications Research.

Corresponding author address: Dr. H. Lee Kyle, NASA/GSFC, Code 636, Greenbelt, MD 20771.

1. Introduction

The Earth's cloudiness plays an important role in the budgets of solar and thermal radiation, and thus on the net radiation in the Earth-atmosphere system. The clouds not only exert a profound influence on long time-scales in determining climate, but also on short time-scales in the development of disturbances through the differential heating between clear and cloudy regions and distabilization of the atmosphere by strong cloud top cooling (Cox 1969; Schneider 1972; Gray and Jacobson 1977). The evolution and distribution of clouds, when coupled with radiative processes, are found to be the most significant factors in the energetics and general circulation of the atmosphere (e.g., Ohring and Clapp 1980; Liou and Zheng 1984).

Recognizing the need for accurate global cloud information for Earth radiation budget studies either as input data in weather and climate model studies that require prescribed cloudiness, or for validation of models that predict cloud configurations (e.g., Melishko and Wetherald 1981; Hansen et al. 1983), the Nimbus-7 Cloud Data Processing Team (CDPT) was formed by the NASA Nimbus-7 Project in late 1982 to produce a global cloud database. The basic measurements are the Nimbus-7 Temperature Humidity Infrared Radiometer (THIR) $11.5\text{ }\mu\text{m}$ radiances and the Total Ozone Mapping Spectrometer (TOMS)-derived $0.37\text{ }\mu\text{m}$ reflectivities. Starting with an earlier IR algorithm (Stowe 1984), the team derived independent IR and UV cloud detection algorithms. The improved IR algorithm uses the THIR radiances together with concurrent surface temperatures from the Air Force three-dimensional nephelanalysis (3DN) archive (Fye 1978), and NCAR climatological atmospheric temperature lapse rates (Jenne et al. 1974). The surface temperature and the atmospheric lapse rates are used to calculate cloud/no cloud, low, middle, and high cloud ($11.5\text{ }\mu\text{m}$) radiance thresholds. The NCAR climatological atmospheric lapse rates are stored in Subtarget Area Geographical Season (STAGS) data tapes by NOAA, and the ($165\text{ km} \times 165\text{ km}$) geographical grid used there also defines the basic grid used in the Nimbus cloud data set. The UV algorithm uses a linear interpolation scheme to estimate cloud amounts from the TOMS $0.37\text{ }\mu\text{m}$ reflectivities. The TOMS $0.37\text{ }\mu\text{m}$ reflectivities are low and relatively uniform for both land and water scenes, which are snow- and cloud-free (Eck et al. 1987). Stowe et al. (1988) determined that on the average the cloud amount varies between 0% and 100% as the TOMS reflectivity varies between 8% and 50%.

The IR algorithm is used both during the day and night, but the UV algorithm can be used only during the day. Further, because clouds and snow are both quite bright at $0.37\text{ }\mu\text{m}$, no UV cloud estimates are made over the snow/ice fields identified by the Air Force 3DN snow/ice analysis. Finally the IR and UV cloud estimates are merged by a bispectral algorithm to produce the new cloud ERB (NCLE) data set.

The NCLE data are then further averaged into the approximately $500 \times 500\text{ km}$ equal target area grid developed for the Nimbus Earth Radiation Budget (ERB) data set (Jacobowitz et al. 1984). Nine subtarget areas are nested in each target area. Results are stored on cloud MATRIX (CMATRIX) tapes. The parameters recorded in both NCLE and CMATRIX data sets include daytime (local noon) and nighttime (local midnight) values of total cloud amount, cloud amount in high, middle, and low altitude categories, cirrus and deep convective cloud amount, and radiances of cloud and clear scenes. The CMATRIX data sets also include the variances of cloud amount and radiance in space (daily) and time (monthly). A detailed description of the algorithm and the error analysis to assess the bias and random errors of this cloud data archive has been reported in Stowe et al. (1988); earlier, a preliminary discussion was given in Stowe et al. (1984). A general description of the data set and its formation can be found in Hwang et al. (1988).

In this paper, we analyze the first year (from April 1979 to March 1980) Nimbus-7 cloud data by presenting three different CMATRIX cloud estimates: ascending node (local noon) IR with and without TOMS data, and descending node (local midnight) IR only. These are compared with other cloud climatologies documented from various sources. Four months of Nimbus-7 cloud data in 1979 and 1980 are selected to represent 4 seasons of cloud climatology. Their zonal and regional characteristics of total cloud amount and distribution of various cloud types are discussed in the following sections. In general, it is found that the Nimbus-7 cloud data are realistic, and meet the requirements of supporting ERB studies. The combination of Nimbus-7 cloud and ERB data (the latter described by Jacobowitz et al. 1984; Kyle et al. 1985) allows the opportunity to study the role of clouds in determining the Earth's radiation budget for a period of 6 years.

2. Nimbus-7 global cloud cover characteristics of the first year data

A 6-year (April 1979 to March 1985) data set has been produced and is available to the scientific community. All of the cloud data passed through a quality control review and short studies have been carried out on portions of the data set (Stowe et al. 1986; Yeh et al. 1986; Ohring et al. 1986; and Hwang et al. 1986). A detailed review of the entire data set is underway. The results of our analysis of the first data year are presented in this paper.

On 24 October 1978 the Nimbus-7 satellite was launched into a circular Sun-synchronous orbit inclined 99.3° to the equator, with a period of 103.9 min. The satellite's altitude is approximately 955 km, and it completes 13.9 orbits per day. It crosses the equator near local noon on the ascending node, traveling from south to north, and near local midnight on the descending node going south. Between 45°N and

45°S lat observations are taken within an hour of local noon during the day and within an hour of midnight at night. Near the poles, the satellite moves parallel to the 80° latitude and quickly traverses several local time hour zones before heading back towards the equator. The subsatellite point never goes beyond latitude 80.7° so that, while some scanning angles view the poles, they never do so near nadir. The Nimbus-7 products are normally produced and stored on a separate ascending node and descending node basis. For most of the globe, these can accurately be described as local noon (AN) and local midnight (DN) data products, or loosely as day and night products.

For several weeks after launch, the THIR and TOMS instruments were shielded to protect them from initial outgassing contaminants. Thus, their observation record of infrared and ultraviolet (UV) radiance data, respectively, begins in November 1978. However, the Air Force surface temperature analysis archive, used by the THIR cloud algorithm, starts on 1 April 1979. Also, the THIR operation was terminated in May 1985, due to a shortage of solar power needed to operate the spacecraft instrument subsystem. Since the THIR was not operated full-time in April and May 1985, it was decided to stop the Nimbus-7 cloud data archive at the end of March. A complete 6-year data set, commencing on 1 April 1979 and ending 31 March 1985 exists.

The spatial and temporal characteristics of monthly mean cloudiness as observed by the Nimbus-7 satellite during the first data year will be discussed in this section. We first discuss the regional and seasonal characteristics of Nimbus-7 clouds as estimated by 1) the THIR/TOMS bispectral algorithm, 2) the THIR-only algorithm for daytime, and 3) the THIR-only algorithm for nighttime. We then illustrate the regional and seasonal characteristics of total cloud, the several cloud types, and cloud radiation.

a. Difference in the three Nimbus-7 estimates

The NCLE and IR cloud algorithms are described in detail by Stowe et al. (1988). In essence, the NCLE is based on a bispectral (0.37 μm and 11.5 μm) algorithm, while the IR algorithm utilizes only the 11.5 μm radiances. The differences between the Nimbus-7 daytime cloud amount estimates with and without the TOMS reflectance estimate (i.e. NCLE and IR) are shown for July 1979 and January 1980 in Figs. 1a and 1b, respectively. These figures show the regional effect of including the reflectance algorithm in the estimate of total cloud amount. The areas where TOMS has added significantly (over 10%) to the IR-only estimate of cloud amount in July are the northern Pacific and Atlantic Oceans, off the west coasts of North and South America and southern Africa, and over most of the Arctic Ocean. These are all areas where low level stratus and/or stratocumulus clouds are prevalent (Hahn et al. 1982). The low level clouds, as previously discussed

in Stowe et al. (1988), are difficult for an IR-only algorithm to detect accurately. The tropical belt in July is the only region where the TOMS estimate reduced the IR-only estimate; rarely is the reduction as great as 10%. The UV estimate is lower than the IR estimate in the tropics due to the presence of cirrus clouds associated with ITCZ convection. When cirrus clouds predominate, the bispectral NCLE algorithm assumes that the IR algorithm slightly overestimates the amount of cirrus present (Stowe et al. 1988).

Figure 1b shows the effect of the TOMS reflectivity algorithm for January 1980. In the Northern Hemisphere there is a large difference between the areas which were modified by TOMS reflectance measurements in July and in January, due to a combination of both cloud altitude and cloud type changes. The major continental areas of North America and Eurasia are the regions where TOMS has added significantly (>10%) to the IR-only cloud amount in January. This is most likely a consequence of high pressure subsidence occurring over these areas which results in a suppression of cloud top height, thus making it difficult to detect these clouds with IR measurements. Another factor which contributes to the difficulty in detecting low altitude cloud with IR measurements over these areas in January is that the vertical temperature lapse rates are relatively small in comparison to the summer. In the Southern Hemisphere in January, the areas where TOMS reflectance measurements have added significantly to the detection of low altitude clouds occurs almost exclusively over the oceans, especially the southern oceans near Antarctica where stratus cloud is predominant, and also off the west coasts of Africa and South America where stratocumulus is the predominant cloud type. It is possible that errors in the snow/ice analysis could contribute to the higher cloud estimates of NCLE over the Northern Hemisphere continents and the Antarctic Ocean. As was the case for July, the tropical regions in January have large areas where the TOMS cloud estimate has slightly reduced the total cloud amount due to the presence of cirrus. The predominant tropical cirrus cloud regions are shown in Fig. 7.

The diurnal variability of cloud amount between local noon and midnight for July 1979 and January 1980 is best shown in Figs. 2a and 2b, respectively, in which the differences between the daytime and nighttime IR-only estimates are plotted. Consistent with the zonal average depiction of these estimates, to be discussed in section 3a, these figures show that, with the exception of a few areas, most of the Earth has more cloud near local midnight than near local noon. The few small areas in July 1979, where the cloud amount at noon is more than 10% greater than at midnight, are on the west and east coasts of tropical Africa and South America. The figures show that the cloudiness over several large land areas, as well as the low level stratocumulus over ocean, tend to be more extensive near midnight than near noon. The negative differences

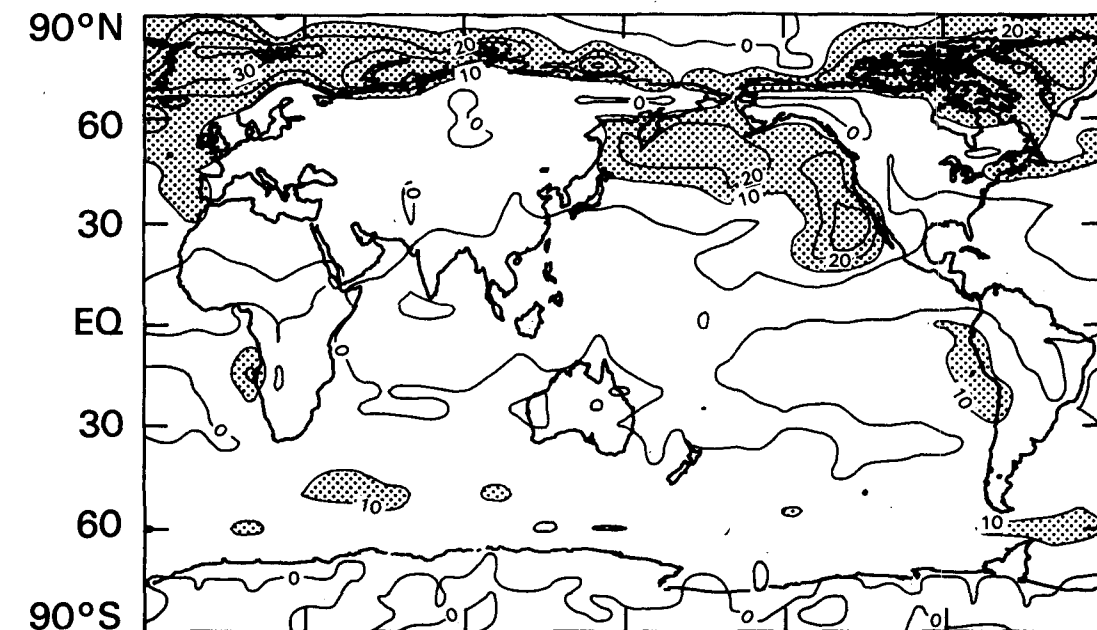
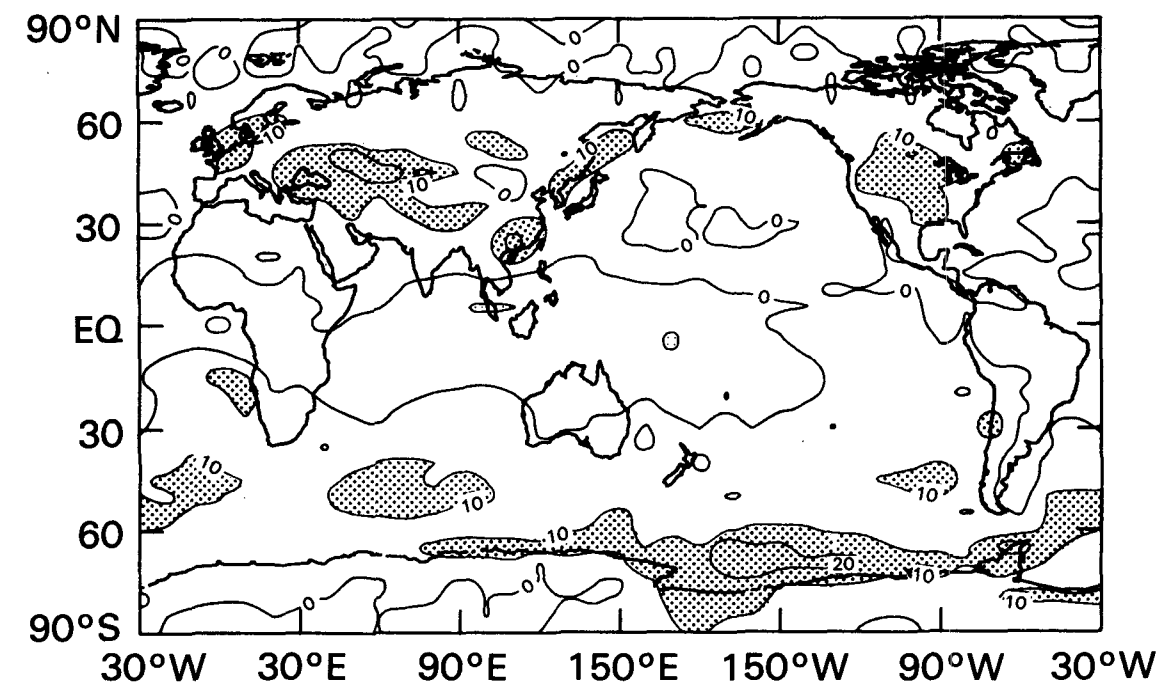
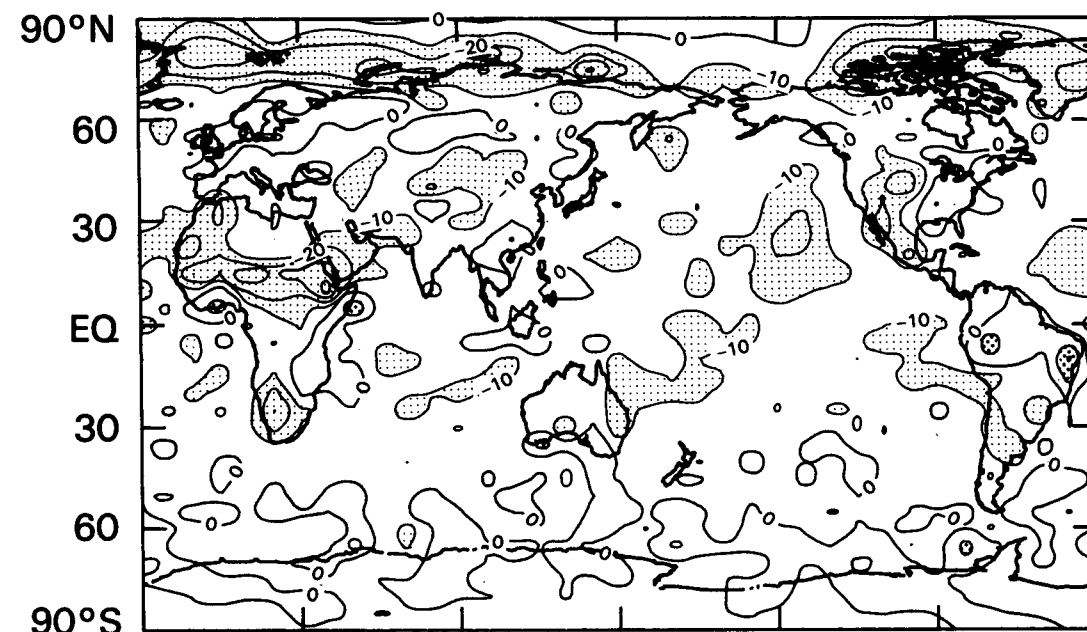
TOTAL CLOUD DAY (W-W/O TOMS) JULY 1979**(a)****TOTAL CLOUD DAY (W-W/O TOMS) JANUARY 1980****(b)**

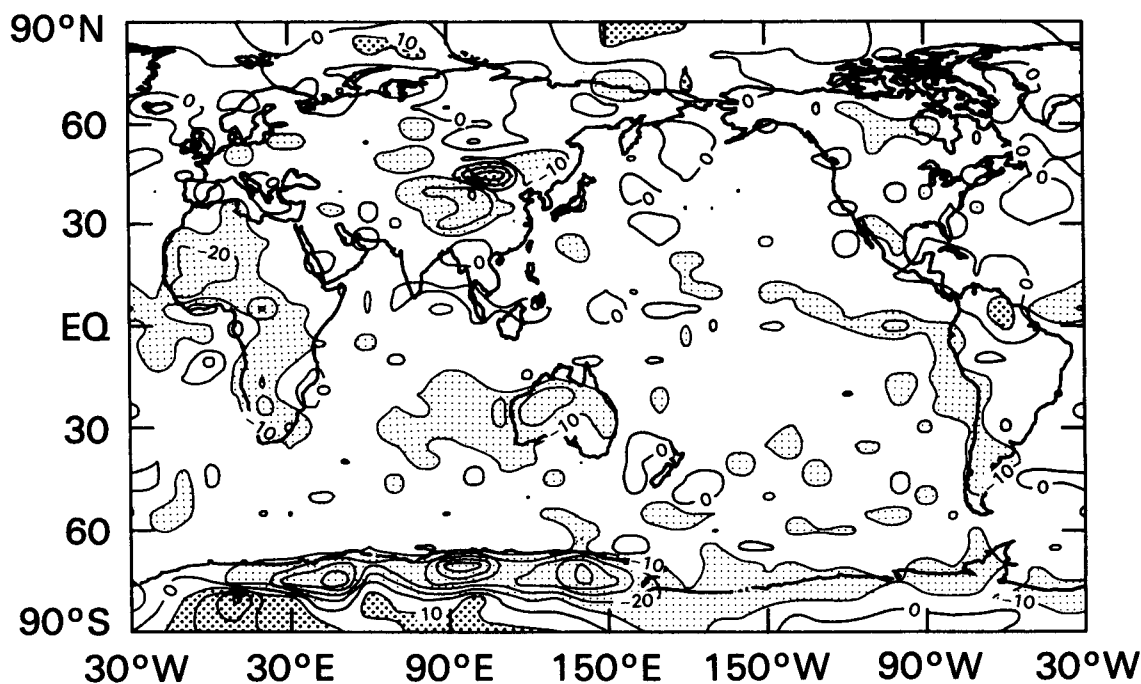
FIG. 1. Difference in total cloud amount (in percent) estimated by the bispectral and IR algorithms in daytime for (a) July 1979 and (b) January 1980. Heavy shaded areas denote more clouds being detected by the bispectral algorithm, and light shading denotes less. Contours are given in intervals of 10%.

TOTAL CLD (DAY W/O TOMS-NITE) JULY 1979



(a)

TOTAL CLD (DAY W/O TOMS-NITE) JANUARY 1980



(b)

FIG. 2. Difference in total cloud amount estimated near local noon (ascending node) and local midnight (descending node), by the IR-only algorithm for (a) July 1979 and (b) January 1980. Heavy shaded areas denote more clouds being detected in daytime, and light shading denotes less.

shown north of 60°N latitude in July are probably not a diurnal effect but rather the result of using TOMS reflectance data on the descending parts of orbits, possible at these high latitudes due to the northerly position of the Sun in July. This negative pattern is almost identical to the positive pattern in this region from Fig. 1, suggesting that if the IR-only descending node estimates were available, they would vary little from the daytime (ascending node) data. This implies that there is very little diurnal variation in cloudiness in the north polar latitudes. In Fig. 2b, large positive differences of 40% to 50% in Mongolia and in the Antarctic may be partially due to algorithm problems associated with difficult retrieval situations perhaps combined with local problems with the 3DN Air Force surface temperatures. The problems in the Antarctic are further discussed in sections 3a and 3b.

Figures 2a and 2b show that total cloud amount at local midnight is greater than that at local noon for the latitude zones between about 40°S and 40°N , particularly over land areas (also evident zonally in Fig. 13). Greater cloud amount at local midnight is physically possible, since on many days convective activity over land occurs in the afternoon and evening hours and these clouds may not have fully dissipated by midnight. Convective processes not only result in greater cloud amount, but also in increasing cloud height, which makes detection of the cloud by an infrared threshold easier, due to the greater temperature contrast with the surface. Most of the difference between the local noon and local midnight cloud amount in the tropics is caused by increasing middle and high cloud at night. This diurnal variation is consistent with the study of Duvel and Kandel (1985), who found from METEOSAT radiance data for the Sahel-Guinea region of Africa (8° – 16°N and 8°W – 22°E) that midlevel cloud (4 to 9.8 km) reaches a maximum between 0300 and 0500 LST and a minimum between 1400 and 1600 LST during the August 1979 wet season. It is noted that the entire north latitude tropical region of Africa in July 1979 is the largest area where the Nimbus-7 algorithm detects greater than 20% more cloud at midnight than at noon.

Another physical mechanism which would result in more cloud amount at local midnight than local noon over the oceans for stratus and stratocumulus cloud types is a diurnal radiative forcing. Hanson and Gruber (1982) have modeled marine stratocumulus and found that the diurnal cycle of solar forcing results in a thinning of cloud during midday when solar radiation is at its peak. This thinning can result in the breakage of a stratocumulus layer with a resulting lower cloud fraction.

Minnis and Harrison (1984) found a diurnal cycle in total cloud for the Amazon River basin (5.6°S , 61.9°W) in November 1978 which shows over 20% more cloud cover at local midnight than at local noon. They identified this diurnal variation to be dominated

by midlevel cloud, defined at the altitude range of 2 km to 6 km. The Nimbus-7 IR algorithm cloud estimates, however, show greater cloud amounts at local noon than local midnight in July for the same area (Fig. 2a), and relatively little variation between noon and midnight in January (Fig. 2b). Thus the diurnal variability of cloud over the Amazon basin may exhibit large seasonal shifts.

There is another factor which could result in the detection of more cloud at local midnight than at local noon by an infrared threshold, even if the cloud amount remained constant. It is the difference between the surface air temperature and the surface skin temperature over arid land surfaces. As discussed in Stowe et al. (1988), the skin temperature (effective infrared radiating temperature) measured by the THIR instrument at local noon typically exceeds the surface air temperature, analyzed by the Air Force, by 20°C or more over large deserts such as the Saharan and Saudi Arabian deserts. Therefore subpixel size clouds or thin cirrus (emissivity $\ll 1$) would be more difficult to detect over land surfaces which have a large skin-air temperature difference. However, the use of TOMS in the bispectral algorithm should substantially correct for this effect. As seen in Figs. 1 and 2, and also zonally in Fig. 13, the NCLE daytime estimate, like the IR daytime estimate, is less than the IR nighttime estimate for latitudes equatorward of 40° , where low altitude clouds and deserts are prevalent. Therefore, it is likely that convection over land and dissipation of marine stratocumulus due to solar heating are the processes responsible for more cloud being observed at midnight than at noon, not the cloud algorithms.

We conclude that, of the three Nimbus-7 estimates, the bispectral algorithm gives the most accurate estimates of daytime cloud amount, but the diurnal variability is best estimated from the differences between day and night values of the IR-only algorithm.

b. Regional and seasonal characteristics of clouds

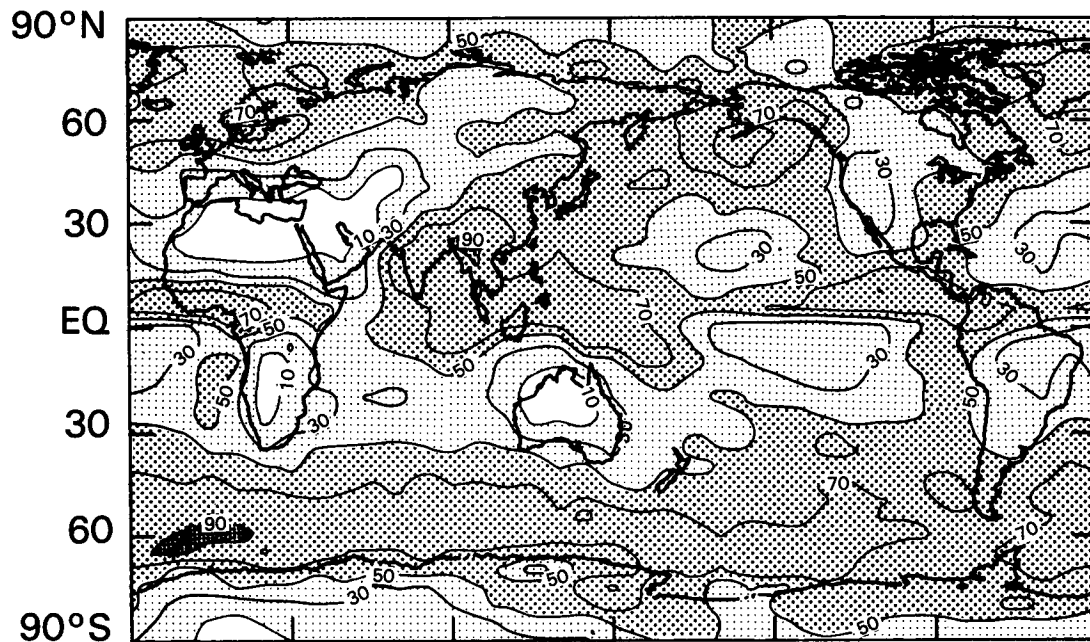
The Nimbus-7 daytime bispectral estimates of July 1979 and January 1980 have been selected to show global cloud patterns during summer and winter seasons of both Northern and Southern Hemispheres in Fig. 3 for total cloud and Figs. 4–8 for different cloud types.

1) TOTAL CLOUD AMOUNT

(i) Northern Hemisphere

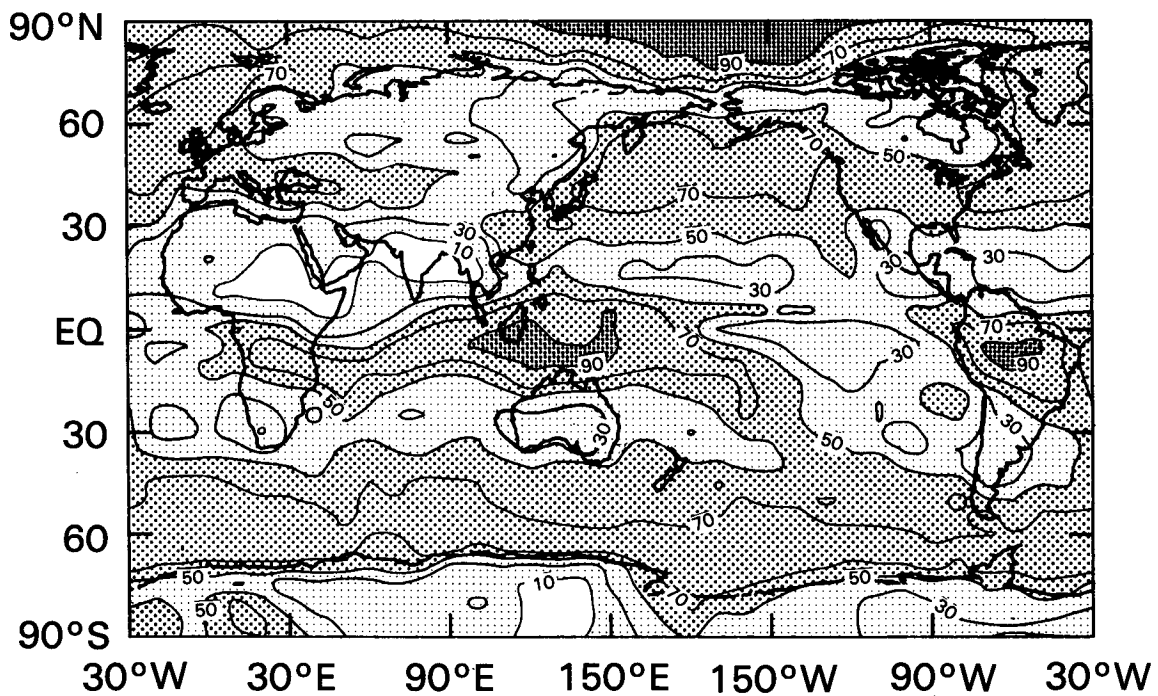
In July, the total cloud amount peaks at about 10°N , close to the mean latitude of the ITCZ, but declines sharply at the latitude of the descending branch of the Hadley cell. The ITCZ is marked by maximum cloud amounts over and near equatorial land areas especially the west coasts of Africa and America, and around India and Southeast Asia ($>70\%$). Over the western

NIMBUS-7 TOTAL CLOUD JULY 1979



(a)

NIMBUS-7 TOTAL CLOUD JANUARY 1980



(b)

FIG. 3. Maps of total cloud amount estimated by the Nimbus-7 bispectral algorithm for (a) July 1979 and (b) January 1980. The contours are for 10%, 30%, 50%, 70% and 90% of cloud fraction. Heavy dots indicate region with cloud amount greater than 90%, medium dots greater than 50%, while light dots indicate amounts between 10% and 50%. Clear is less than 10%.

Pacific Ocean, the ITCZ is also marked by a persistent maximum cloud zone. The prevailing cloud cover (>90%) associated with the Asian monsoon is obvious. The cloudiness of this area in July exceeds that of any other convective cloud region.

The minimum cloudiness is related to the subtropical high pressure subsidence which occurs just north of the ITCZ. The most apparent cloud amount minima in summer (July) is situated over the Northern African and Middle Eastern deserts (<10%) and western United States (<30%). Semipermanent high pressure spreads over most of the Pacific and Atlantic oceans, south of 40°N. Consequently, large portions of the oceans are less than 50% cloud covered.

In winter (January), the subtropical high pressure areas move southward, close to the equator, so the midlatitude cloud minima also moves to lower latitudes. The cloud amount off the west coasts of the North American and European continents increases substantially in January, probably because these are regions often affected by winter storms, and their associated cloudiness. At the middle and high latitudes of the North Pacific, the most severe weather of the year generally occurs in January. The circulation over the Pacific Ocean is mainly controlled by the major centers of action: the Aleutian low, the subtropical high, and the Siberian and Canadian highs which are all near their peak seasonal development. The related cloudiness in January is extensive, especially so over the northwestern Pacific Ocean. The Nimbus-7 cloud amount estimates in the Arctic are less reliable than those at lower latitudes for several reasons. This is discussed in section 3a where a comparison is made with the results of other investigators.

(ii) *Southern Hemisphere*

In the summer month (January), the ITCZ is situated south of the Equator, and extensive cloudy areas appear at the 10°S latitude zone. The cloud amount maxima (>90%) occurs over Brazil and to the northwest and north of Australia. This finding agrees with the results from Air Force 3D-nephanalysis for January 1979 (Henderson-Sellers and Hughes 1985). The minimum cloud amount (<50%) located in oceanic regions extending to almost 40°S is associated with subtropical high pressure systems.

The coastal stratus off the west coast of South America and Africa is prevalent in July (winter), with large areas in which the cloud amount exceeds 50%. The UV reflectivities from TOMS have undoubtedly helped in the identification of low level and relatively warm coastal stratus (Fig. 1a). Also, the equatorward advances of clouds associated with increased polar front activity is particularly noticeable in the South Pacific Ocean.

The Nimbus-7 cloud cover data over Antarctica should be used with caution. A comparison with the

results obtained by some other investigators is given in section 3a.

2) LOW, MID, HIGH, CIRRUS, AND DEEP CONVECTIVE AND WARM CLOUD AMOUNTS

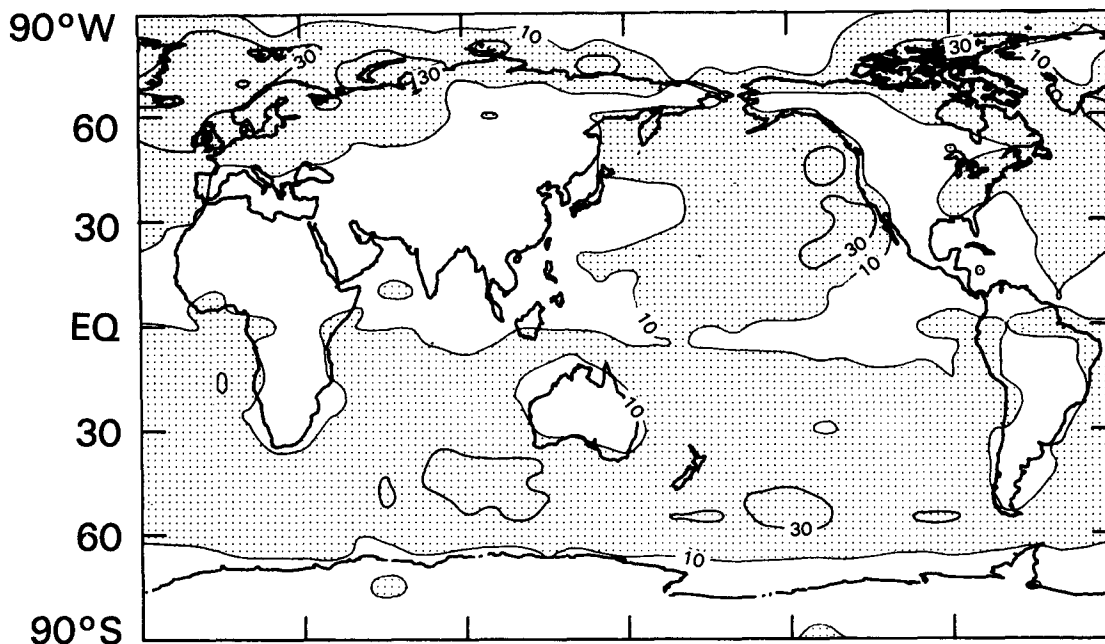
(i) *Low cloud amount for July 1979 and January 1980*

The geographical distribution of low cloud amount for July 1979 is shown in Fig. 4a. Most of the ocean areas in July have 10%–30% low cloud amount with the exception of the equatorial oceans from approximately 5°S to 20°N which have less than 10% for several extensive regions. These areas are the most active regions of the ITCZ, extending from the eastern Pacific through the northern tropical Atlantic and into the Atlantic Ocean, across Indonesia and into the western tropical Pacific. The lesser amounts of low cloud detected in this ITCZ region is due in part to the masking of the lower layer of clouds by the large amounts of overlying mid and high clouds (Figs. 16 and 17). This masking of low level clouds also occurs in many land regions in the ITCZ, notably the Indian subcontinent, Southeast Asia, Central America, and northern South America. Since surface level moisture reaches high levels in the ITCZ region, it would be likely that conditions for the formation of low clouds would be favorable.

Seze et al. (1986) compared surface observers estimates of cloud with estimates made by using a clustering technique which input radiance measurements made by the METEOSAT satellite. They found that, when there were multilayer clouds in the study area of France and southern Britain, the satellite retrieval tended to underestimate low cloud amount relative to a surface observation. They concluded that this was because the satellite view of the low cloud was obscured.

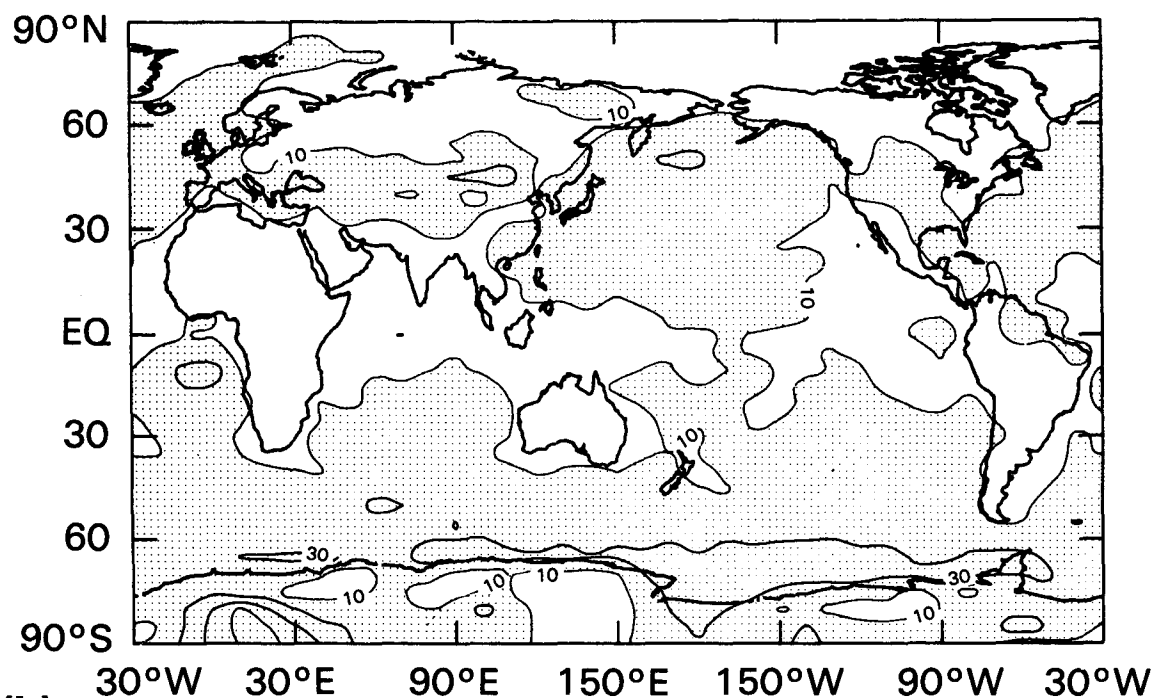
Over the large majority of continental land masses in July, the low cloud amount is <10%, which is in general less than most ocean areas outside the tropics. This is probably due to the lack of a surface level moisture source which is necessary for the formation of most low level cloud. The notable exceptions are the Amazon River Basin, some of the rainforest areas in equatorial Africa, eastern North America, and most of Europe and the western U.S.S.R. The higher amount of low level cloud detected over the Amazon is due to both a relatively small amount of mid and high cloud in this region which would overlay the low cloud, and also due to the moisture source of the actively transpiring rainforest. The relatively large amount of low cloud in eastern North America is due to the northward flow of moist warm air from the Gulf of Mexico up through New England, and north of that region possibly due to the large amounts of lakes and bays in eastern Canada combined with moisture from the Hudson Bay. Over Europe the prevailing surface winds in July are from the Atlantic and Arctic Oceans.

NIMBUS-7 LOW CLOUD JULY 1979



(a)

NIMBUS-7 LOW CLOUD JANUARY 1980



(b)

FIG. 4. As in Fig. 3 except for low cloud.

Areas of maximum low cloud amount ($>30\%$) in July occur only over oceans. In the Pacific off the west coast of North America, they are most likely stratocumulus. Other low cloud maxima also prevail in the northeastern Atlantic, and in the southern Pacific from about 35° to 55°S .

As in July, the oceans in January (Fig. 4b) are predominantly covered by 10% – 30% low cloud amount. Again, the equatorial areas of minimum oceanic low cloud amount coincide with areas of large amounts of mid plus high clouds. The global maximum amount of low level cloud over land ($>30\%$) occurs in Mongolia, which is a strong center of surface high pressure in January. This high pressure and associated subsidence of air would limit the vertical development of clouds and possibly be the cause of low cloud predominance. The oceans areas with maximum cloud amount in January include the area immediately south of the Aleutian Islands in the Northern Pacific and the region of stratocumulus cloud off the west coast of southern Africa.

Henderson-Sellers (1986) studied the layer cloud amounts from the U.S. Air Force 3D-Nephanalysis (3DN) for July and January 1979, using the same definition for low cloud (0–2 km) as the Nimbus-7 climatology. The layer cloud amounts in the 3DN do allow for overlap of cloud amount in different cloud layers for a given observation time by the inclusion of surface and aircraft reports, while the Nimbus-7 cloud retrieval allows only for the detection of the highest altitude level clouds for a given observation. Therefore, direct comparison of layer cloud amount magnitude is not possible between the two climatology data sets, but a comparison of areas of relative maximum and minimum amounts is useful. For July 1979 both the 3DN and Nimbus-7 show minimum of low cloud amounts in western North America, most of South America, the Sahara and middle eastern deserts extending into central Asia, southern Africa, and Australia. The most striking difference between these two climatologies is the large amount of low cloud associated with the ITCZ (61% – 80%) for the 3DN while, as mentioned previously, the Nimbus-7 low cloud amount for much of the ITCZ region is less than 10% . The 3DN shows the low cloud layer as the dominant cloud layer in the ITCZ in July while the opposite is true for the Nimbus-7 climatology. It seems unlikely that the fact that the Nimbus-7 does not detect underlying low clouds would account entirely for the large differences, which are possibly also due to other fundamental algorithm differences.

(ii) *Middle cloud amount for July 1979 and January 1980*

Figure 5a shows the geographical distribution of midlevel cloud for July 1979 for local noon. The areas of maximum middle cloud amount ($>50\%$) include

the ITCZ regions of equatorial west Africa, northern South America, and the eastern equatorial Pacific at about 10°N . Other areas where middle cloud exceeds 50% include the wet monsoon regions of India and Southeast Asia, and the extensive stratocumulus cloud areas located off the coast of Peru and in the Atlantic off the coast of South Africa. Stratocumulus are usually thought of as low level clouds; however, the mid cloud altitude range for the Nimbus-7 climatology is 2–7 km for 30°N to 30°S . Therefore, stratocumulus could easily be classified as midlevel cloud (cf section 3b). Large amounts of midlevel cloud ($>50\%$) also occur from 50° – 60°S associated with the Antarctic polar front. The minimum amounts of midlevel cloud ($<10\%$) occur over the ocean in the subtropical high pressure centers which are associated with the descending branches of Hadley cell circulation. Over land, minima are common in desert regions.

The midlevel cloud amount of the 3DN for July 1979 is in general agreement with Nimbus-7 midlevel cloud amount for some areas, notably the ITCZ region from the central Pacific to the east coast of Africa. Other regions which show middle cloud maxima in both climatologies are the southeastern United States, northeastern Canada, most of Europe except Spain, and the large area from India through southeast Asia including Indonesia, and extending into the western Pacific. Areas where there are large discrepancies between the 3DN and Nimbus-7 in July 1979 are the regions of stratocumulus off the west coasts of the United States, Peru, and southern Africa. The largest difference occurs off the west coast of southern Africa where the Nimbus-7 middle cloud estimate is 50% – 70% cloud while the 3DN shows only 0% – 20% . The discrepancy may be due to the fact that these clouds are close to the low/mid cloud boundary definition and are being classified as low level by the 3DN.

Comparing January 1980 Nimbus-7 middle cloud amount (Fig. 5b) with July 1979, the areas showing the largest change are the monsoon regions of India, Southeast Asia, and the Amazon Basin. These changes are largely due to the southward movement of the ITCZ. In both India and Southeast Asia, the middle cloud exceeds 50% for large areas in July 1979, while in January 1980 the middle cloud amount is less than 10% . The monsoon regime in the Amazon, which is south of the equator, is similar to the northern tropical monsoons, but here the maximum middle cloud amounts of 50% – 70% occur in January. Other extensive regions of large middle cloud amount occur in the northwest Atlantic, associated with the Labrador low, and at 60°S extending from 30°W to 45°E , associated with the Antarctic polar front. Minimum cloud amounts ($<10\%$) over the oceans in January occur mostly in the subtropical high pressure areas which are generally smaller in extent than in July. An area of minimum mid cloud ($<10\%$) also extends from Mongolia through Siberia. This may be due in part to the

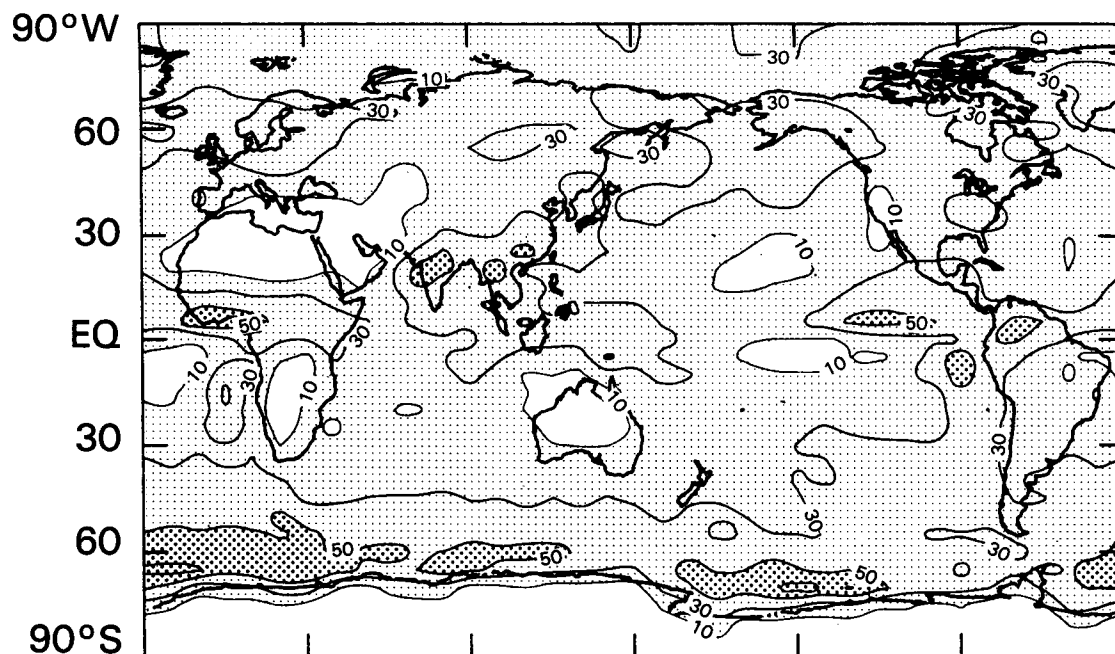
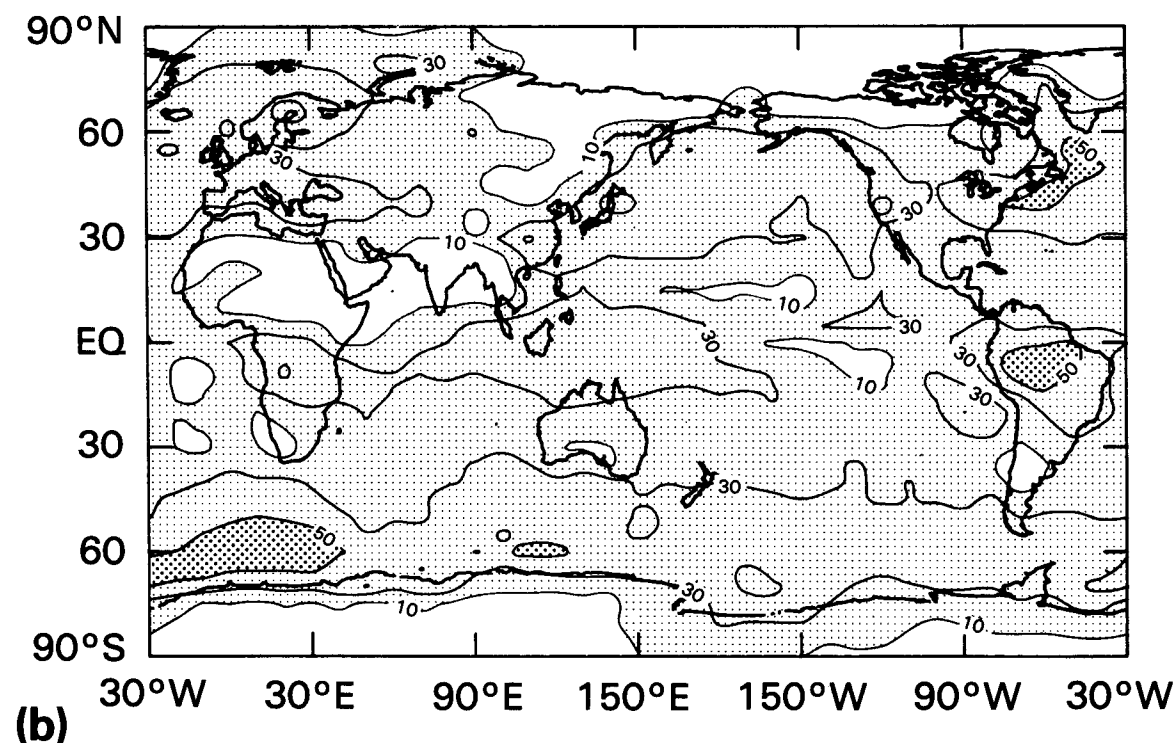
NIMBUS-7 MIDDLE CLOUD JULY 1979**(a)****NIMBUS-7 MIDDLE CLOUD JANUARY 1980****(b)**

FIG. 5. As in Fig. 3 except for middle cloud.

presence of high pressure systems which suppress cloud vertical development, as was noted in the previous discussion of low cloud, which has a regional maximum there. It is also observed that the large areas of stratocumulus clouds in July off the coast of Peru and in the Atlantic off of South Africa have diminished greatly in January. Both the 3DN and Nimbus-7 show an intrusion of midlevel cloud into the southwestern Sahara region (20%–40% and 10%–30%, respectively) in January. For the rest of the Sahara across southern Saudi Arabia into India and Southeast Asia, the middle cloud amounts are at a minimum.

(iii) *High cloud amount for July 1979 and January 1980*

The global distribution of high cloud amount for July 1979 at local noon is shown in Fig. 6a. The major global high cloud feature is the ITCZ region and the areas of maximum high cloud amount are in the Indian and Asian monsoon regions. Outside of these areas, the only significant region where high cloud exceeds 30% is in the Pacific, adjacent to Japan. High cloud minima occur in the central and eastern midlatitude North Pacific extending into western North America, the central and eastern North Atlantic extending into North Africa, Europe, and the Middle East. High cloud amount is also less than 10% for most of the latitude zone between 30°S and the equator except for Indonesia and the Indian Ocean south of the monsoon regions.

Barton (1983) developed an upper level cloud climatology for clouds higher than 6 km using radiation measurements from two narrow-band, near-infrared channels (in the 2.7 μm region) of the Selective Chopper Radiometer on Nimbus-5. His cloud distributions are only representative of high cloud amount in the tropics and midlatitudes of the summer hemisphere, since, for other latitudes, there are significant errors due to high solar zenith angles and the lower altitudes of clouds due to decreasing tropopause height. Barton's cloud retrieval technique enables the sensing of high altitude cloud without concern about radiation contributions from the surface and lower level clouds, and therefore can determine the amount of high cirrus clouds reasonably well.

A comparison of Barton's high cloud amount for June, July, August (1973 and 1974 average) with Nimbus-7 high cloud amount shows very good agreement in regional distribution between the two separate estimates. The magnitudes of Barton's high cloud amounts, however, are generally about 10% greater than the Nimbus-7 high cloud amounts. This difference in magnitude may be due in part to the misidentification of some thin high cirrus as midlevel cloud by the Nimbus-7 algorithm and also due to the difference in the high cloud altitude definition which is 7 km in

the tropics for Nimbus-7 versus 6 km for Barton's climatology.

The high cloud amount determined by the 3DN (Henderson-Sellers 1986) for July 1979, also agrees fairly well with the Nimbus-7 estimates both in regional distribution and approximate magnitude. Both of these climatologies have the same areas of maximum high cloud amount, southern Central America and the adjacent Pacific, parts of Southeast Asia, Indonesia, and the Philippines. Henderson-Sellers (1986) states that the 3DN also tends to underestimate the altitude of high clouds with emissivity of less than one (e.g., thin cirrus) classifying them as midlevel clouds. In addition, the latitudinally invariant definition of the middle/high cloud boundary in the 3DN tends to classify polar latitude high cloud as mid cloud. High cloud distributions over polar regions will be further discussed in section 3b.

For January 1980, the Nimbus-7 high cloud amounts for local noon (Fig. 6b) show a less well-defined ITCZ than for July 1979. In particular, there is a large gap in the ITCZ across the central and eastern south equatorial Pacific, where high cloud amount is less than 10%.

This is consistent with NOAA satellite measurements of outgoing longwave flux as found by Hartmann and Recker (1986). Their study suggests that there are fewer deep convective clouds and more clear sky occurrences during the December, January, February (DJF) season in the Pacific ITCZ than in the June, July and August season, and that the ITCZ is normally very weak in DJF except during an El Niño event. The latitude zone of the descending branch of the Hadley cell in the Northern Hemisphere ($\sim 10^\circ$ – 30°N) has, for the most part, less than 10% high cloud. The areas of maximum high cloud amount ($>30\%$) in January 1980 are the monsoon area of Brazil, a band extending from central and eastern Africa to the large area of deep convection encompassing all of Indonesia and extending into the south central Pacific. The only areas with high cloud amount $> 50\%$ lie between Australia and Indonesia, and in the Arctic Ocean.

As in July, there is close agreement between the Nimbus-7 January 1980 high cloud distribution and Barton's (1983) high cloud climatology for December, January and February for the tropics and the southern midlatitudes. Again the magnitudes of Barton's high cloud amounts are roughly 10% greater than Nimbus-7, especially in the region encompassing Indonesia to northern Australia and into the western Pacific.

High cloud amount from the 3DN for January 1979 (Henderson-Sellers 1986) is also in general agreement in location and magnitude with Nimbus-7, except for the region of Nimbus-7 maximum high cloud amount. In this region, immediately to the south of Indonesia, the Nimbus-7 high cloud amount is greater than 50%, while the 3DN shows mostly 21%–40% for this area. The reasons for the difference are not known, but in-

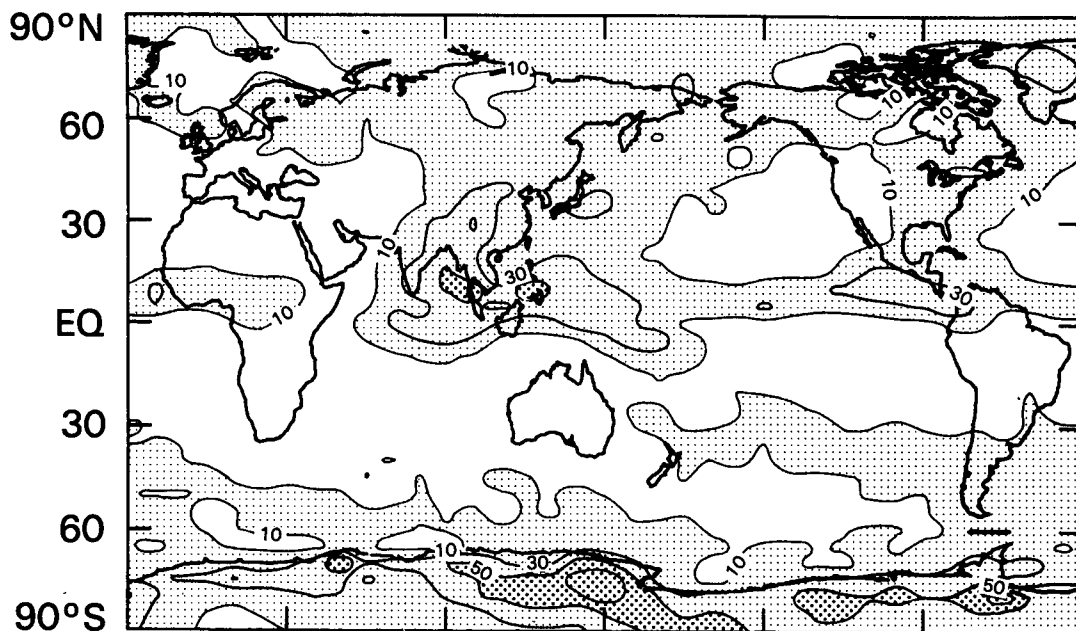
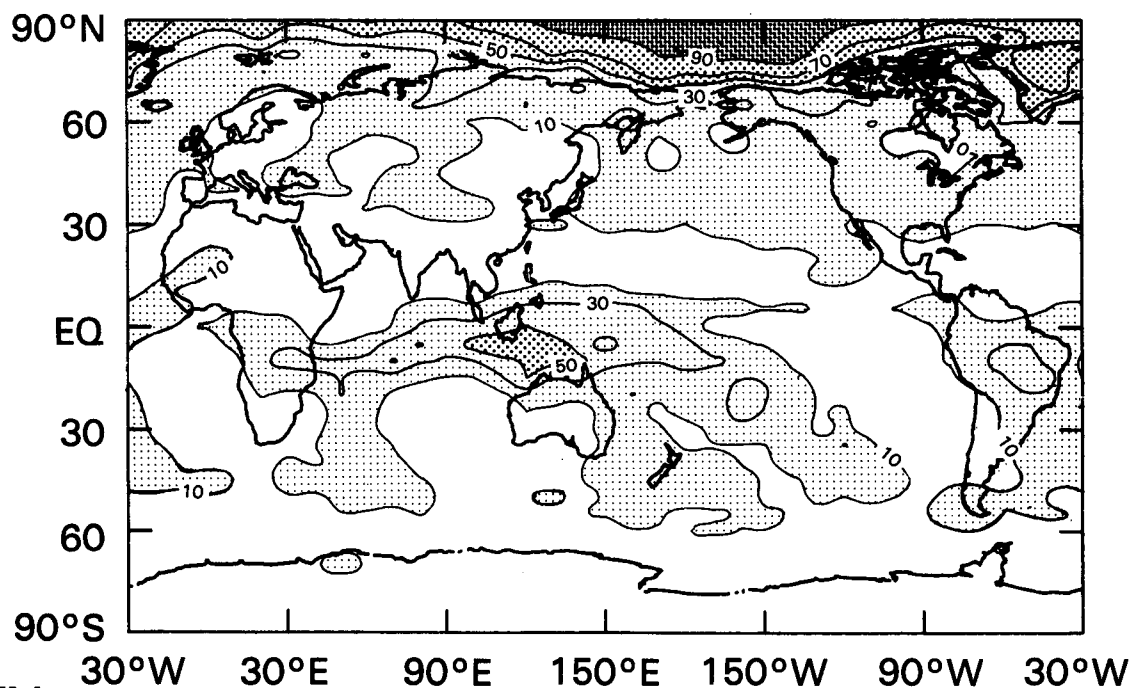
NIMBUS-7 HIGH CLOUD JULY 1979**(a)****NIMBUS-7 HIGH CLOUD JANUARY 1980****(b)**

FIG. 6. As in Fig. 3 except for high cloud.

terannual variability in addition to algorithm differences are possible factors.

(iv) *Cirrus cloud amount for July 1979 and January 1980*

A subset of cold (IR) mid and high clouds, appearing relatively dark in the UV, is termed "cirrus," during the comparison and blending of the Nimbus IR and UV cloud amount estimates (Stowe et al. 1988). The Nimbus-7 can detect cirrus clouds only during daylight and when there is no underlying cloud or snow.

The region of maximum cirrus amount detected by the Nimbus-7 algorithm in January 1980 is in the Indonesian region, extending westward into the Indian Ocean and eastward into the Pacific (Fig. 7b) where cirrus cloud percentage ranges from 10%–25%. Other areas where cirrus cloud is detected include southeastern Brazil extending across the Atlantic into sub-Saharan Africa and southern tropical Africa. An analysis of ship report observations by Hahn et al. (1982), of the frequency of occurrence of cirriform clouds for December–February 1965–1976, shows a close correspondence of regions of maximum frequency of occurrence over oceans with Nimbus-7 cirrus cloud percentage. For example, the maximum frequency of occurrence of cirriform clouds observed by ships occurs over and south of Indonesia at 0°–15°S with 53%–54% frequency of occurrence, which is also the most extensive region of maximum cirrus cloud amount over oceans from the Nimbus-7 algorithm. Areas where the frequency of occurrence of cirrus from ship reports is high but the Nimbus-7 cirrus fraction is low include a large area of the Pacific off of the western United States, and an extensive region in the North Atlantic where frequency of occurrence is >30%, while Nimbus-7 cirrus fraction is <5%.

Similar to the January cirrus distributions, the July 1979 global oceanic maximum (Fig. 7a) of Nimbus-7 percent cirrus cloud (10%–20%) coincides with the maximum frequency of occurrence of cirrus from ship reports for June, July and August (50%–60%) for the region of southeast Asia and the Bay of Bengal. Also there is agreement about a local maximum in the equatorial Pacific immediately to the west of Central America where the Nimbus-7 detects 10%–20% cirrus and the ship observations show 53% frequency of occurrence. Major areas of disagreement between the analysis of ship observations and the Nimbus-7 estimates in July 1979 are the North Atlantic and North Pacific where the frequency of occurrence from ships is 40%–45% while the fraction of cirrus from Nimbus-7 is less than 5%. It must be recognized that these two parameters (cloud fraction and frequency of occurrence) are not the same, and also that the Nimbus-7 algorithm detects cirrus only when there are no or very few other clouds present. By contrast, the ship observers can detect cirrus for cases where there are breaks or

gaps in low level clouds and thus can identify the presence of cirrus in some situations where the Nimbus-7 satellite algorithm cannot.

(v) *Deep convective cloud amount for July 1979 and January 1980*

Another Nimbus-7 subset of cold (IR) high cloud, appearing very bright in the UV, is termed "deep convective" (Stowe et al. 1988). The deep convective cloud percentages in January 1980 (Fig. 8b) are lower than cirrus cloud percentages in the ITCZ (Fig. 7b), probably due to less persistence in time for a given location and to the smaller areal extent of deep convective cells versus cirrus cloud layers. The Nimbus algorithm has detected a band of deep convective cloud ranging from 5%–15% in the ITCZ region between Indonesia and northern Australia and extending into the Indian Ocean to the east coast of Africa. This area is also the maximum frequency of occurrence of cumulonimbus (Cb) from ship reports (Hahn et al. 1982) which ranges from 20%–23%, and is also considerably less than the frequency of occurrence of cirrus observed by ships. Also, there is general agreement between Cb frequency of occurrence from ships and the Nimbus-7 estimates for the local maximum in the Atlantic off of southeast Brazil. Other areas of deep convective clouds identified by Nimbus-7 are located in the North Pacific in the region of the Aleutian low, from the Gulf of Mexico up the east coast of North America and into the North Atlantic and the South Indian Ocean southeast of southernmost Africa. The eastern United States/North Atlantic region is a major storm track, with cyclogenesis occurring adjacent to the Gulf of Mexico and near Cape Hatteras. All of these areas have fairly low frequency of occurrence of Cb (6%–10%) from ship observations. Hahn et al. (1982) and Warren et al. (1985) have computed the probability of simultaneous occurrence of different cloud types. They have found that for December–February (1965–1976) the probability of simultaneous occurrence of cirrus and nimbostratus (precipitating stratus) is maxima over the Indian Ocean southeast of South Africa (56%), the North Pacific (19%–39%) and over the western North Atlantic (29%). These are the same areas where the Nimbus-7 algorithm detected large amounts of deep convective clouds. Thus, Nimbus-7 may be classifying thick stratus (with embedded Cb cells) with overlying cirrus cloud as deep convective cloud in these regions since it is fairly typical for extratropical cyclonic systems to have an overlying cirrus shield (Hobbs 1981).

In July 1979 (Fig. 8a) there is an extensive area of deep convective activity with 5%–15% cloud amount associated with the ITCZ in the eastern Pacific and the monsoon in Southeast Asia. Part of this monsoon area (eastern) is the region of maximum global frequency of occurrence of cumulonimbus clouds (20%–23%) observed by ships. The ITCZ region west of Central

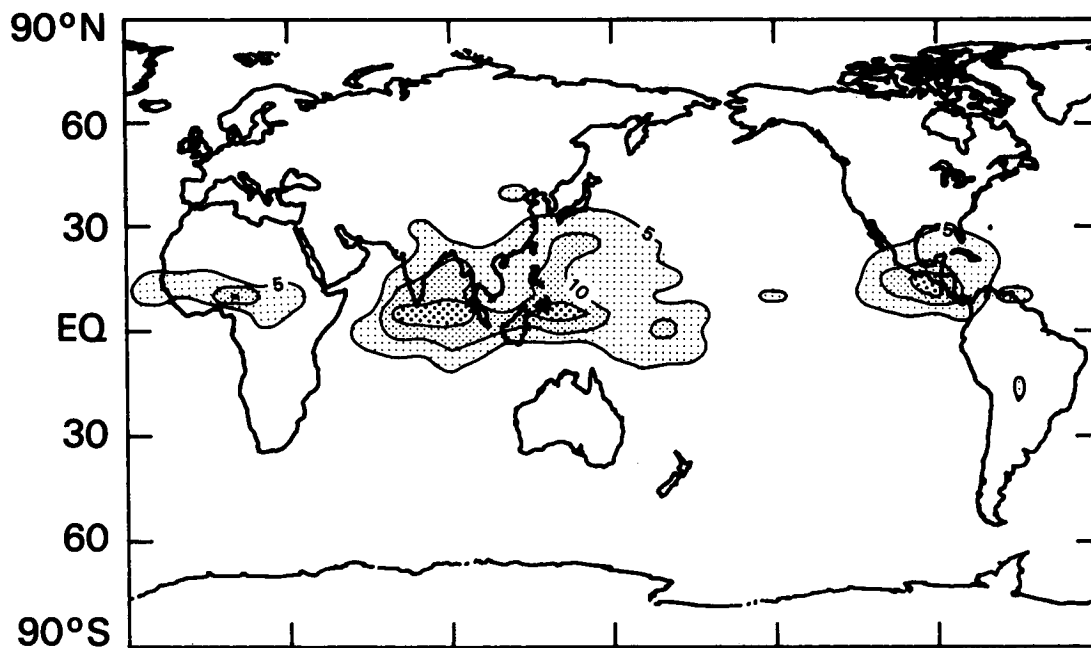
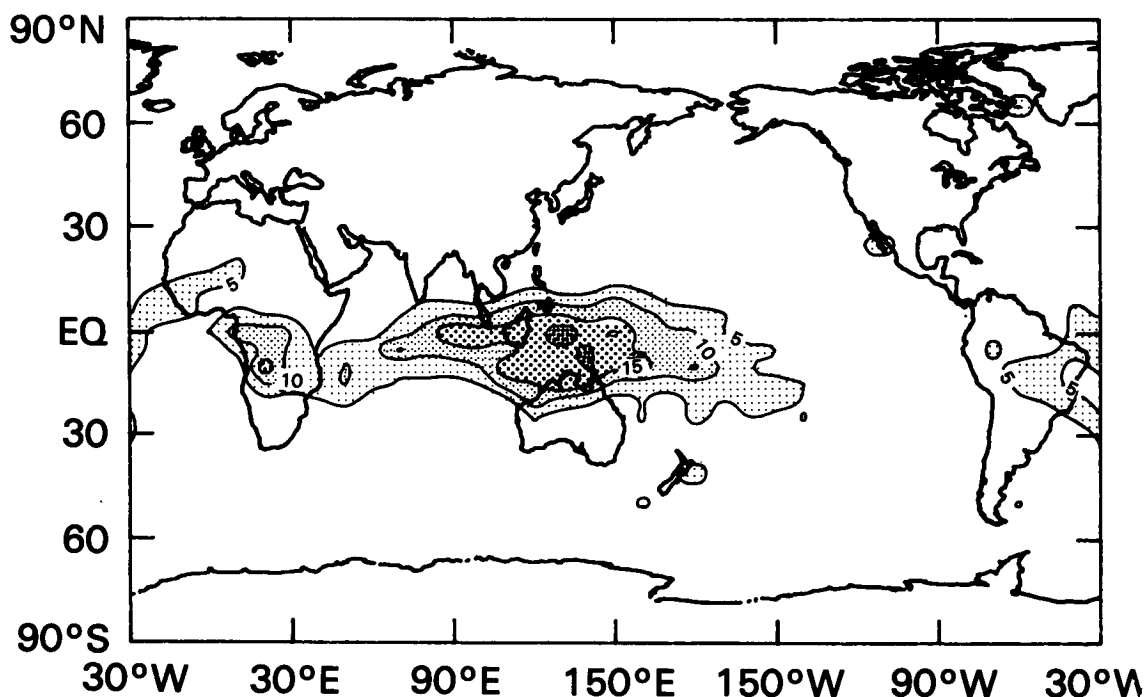
NIMBUS-7 CIRRUS CLOUD JULY 1979**(a)****NIMBUS-7 CIRRUS CLOUD JAN 1980****(b)**

FIG. 7. Maps of cirrus cloud amount estimated by the Nimbus-7 bispectral algorithm for (a) July 1979 and (b) January 1980. The contours are drawn at 5% intervals.

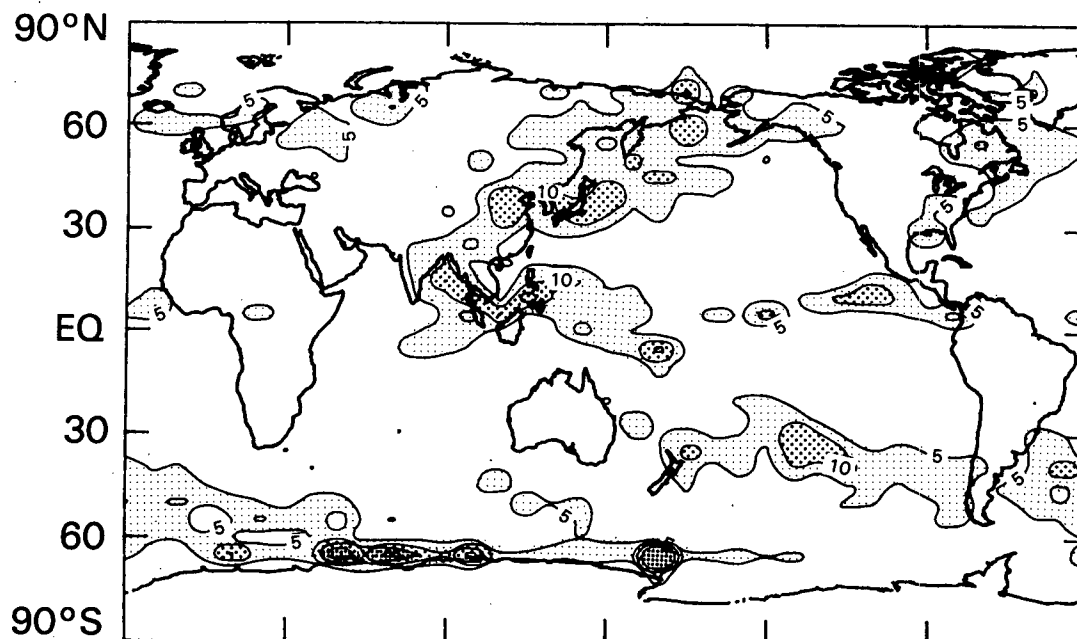
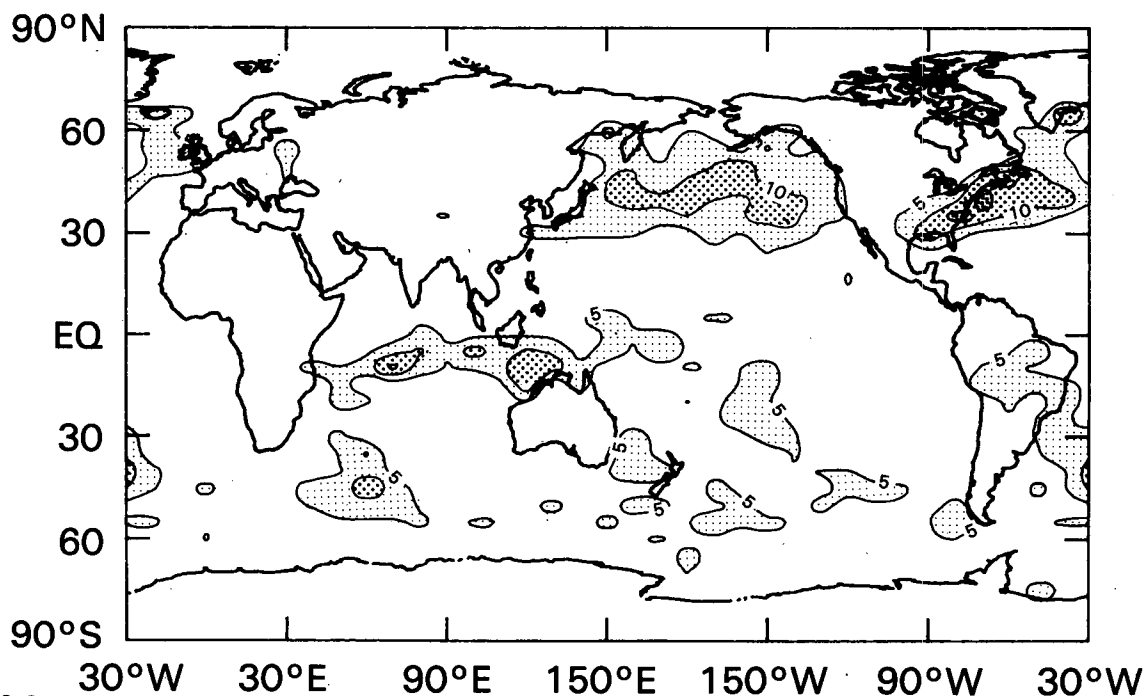
NIMBUS-7 DEEP CONVECTION JULY 1979**(a)****NIMBUS-7 DEEP CONVECTION JAN 1980****(b)**

FIG. 8. Same as Fig. 7 except for deep convective cloud amount.

America to the midPacific is another area where there is both a maximum in Cb observed by ships (15%–19%) and a maximum in deep convective cloud (5%–15%) detected by Nimbus-7. The area of deep convective cloud identified by Nimbus-7, which is adjacent to the Antarctic continent from about 0°–180°E, is most likely due to the presence of cirrus cloud over the ice shelf of Antarctica and the inappropriate use of TOMS data due to errors in the Air Force snow/ice data set there. In this case since ice is not identified, the high reflectance measured by TOMS and the low temperature of the cirrus measured by THIR would therefore result in the misidentification of deep convective cloud. The areas of deep convective maxima identified by the Nimbus-7 algorithm over the Pacific east of Japan and adjacent to the northeastern most extension of Siberia near the Bering Strait are found to be regions of low frequency of occurrence of Cb (2%–7%) from ship reports. However, these areas have both high frequency of occurrence of stratus/stratocumulus (48%–77%) and high frequency of occurrence of cirrus (41%–45%) from ship reports. Hahn et al. (1982) have found that for June–August (1965–1976) the area of maximum probability of stratus being present given that cirrus is present is maximum over the central North Pacific (54%–65%). The Nimbus-7 deep convective cloud algorithm can misidentify this multilayer cloud with overlying cirrus as deep convective since the radiative properties of these clouds could have both high reflectivity and low effective radiative temperature. From ship reports it is found that (Hahn et al. 1982), given the occurrence of cirrus cloud, the probability that nimbostratus is also present is at a regional maximum in the south central Pacific (18%) for 30°–45°S and 120°–150°W, which coincides with a large region of deep convective cloud identified by the Nimbus-7 algorithm.

(vi) *Warm clouds*

At times, the observed 11.5 μm IR radiative temperature (radiance converted into equivalent blackbody temperature) is noticeably larger than the reported Air Force surface temperature. Over the oceans the Air Force temperatures are derived from surface temperatures, but over land they come from shelter temperatures. Near noon (the Nimbus-7 observing time), in hot arid regions the actual surface temperature can be more than 20°C greater than the shelter temperature. However, unusually warm radiances are also frequently observed in cool regions where low altitude atmospheric temperature profile inversions are known to be common. Thus, as described in Stowe et al. (1988), the Nimbus-7 cloud algorithm calculates both a cold and a warm cloud/no cloud threshold. If the observed radiative temperature is greater than the warm threshold, and the climatological temperature profile has an inversion, the algorithm estimates the amount of warm

cloud. However, this is done only if the Air Force surface temperature is below 280 K. This additional requirement prevents the algorithm from incorrectly reporting warm noontime clouds over hot desert regions. These warm clouds are not identified separately in the data set, but can be identified as low clouds with temperatures (radiances) greater than the clear-sky value.

Figure 9a shows the reported warm clouds during July 1979. They occur, in relatively low amounts, over Greenland in the Northern Hemisphere and over the Antarctic continent in the Southern Hemisphere. However, in January (Fig. 9b) warm clouds are fairly numerous at high latitudes over the cold continental land masses in the Northern Hemisphere. The largest concentration occurs in northeast Asia where 10% to 25% of warm clouds are observed. Comparison of Fig. 9b with the previous cloud maps indicates that a large percentage of the winter clouds in this region appear as warm clouds.

Cloud data sets do not commonly identify a separate “warm cloud” category. Thus, there is very little data with which to compare. All that can be said is that the Nimbus-7 warm clouds normally occur where warm clouds are frequently reported by surface observers at the altitude’s temperature inversions.

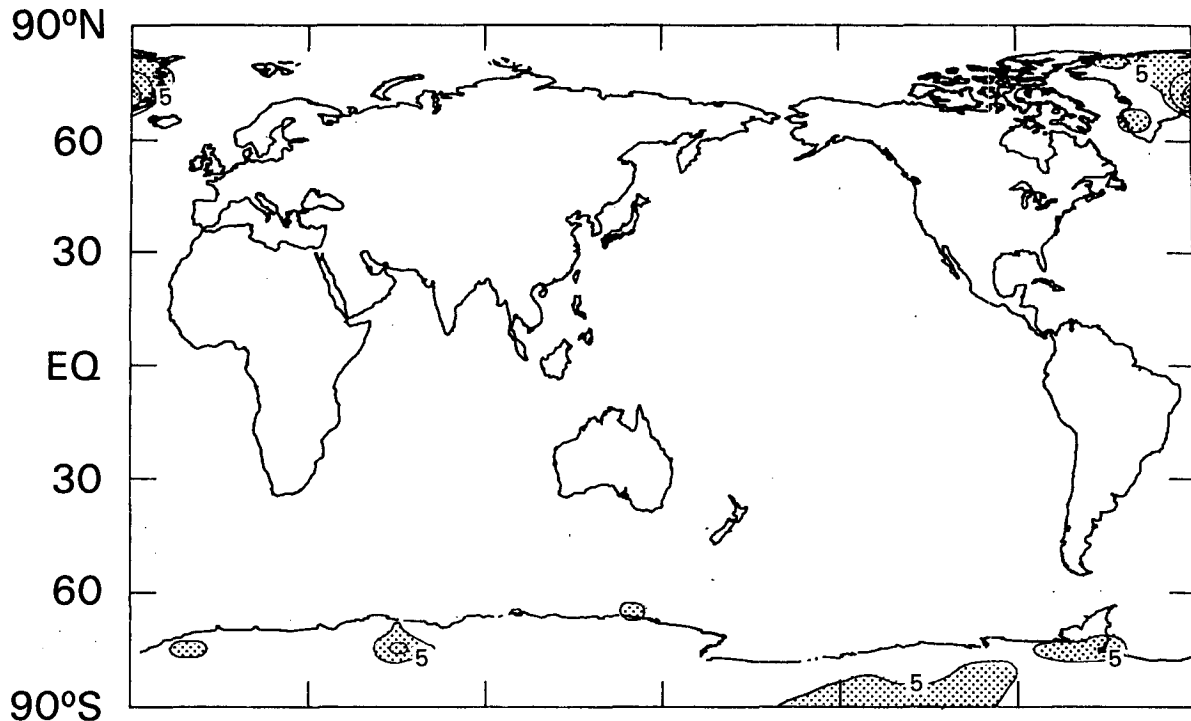
3) CLOUD RADIATION

Target area zonal means of total scene 11 μm IR radiative temperature (radiance converted into equivalent blackbody temperature)¹ and the corresponding TOMS UV reflectivity for July 1979 and January 1980 are shown in Fig. 10. The total scene IR temperature scale is on the right-hand side, and the UV reflectivity scale is on the left-hand side of the figure. The total scene temperatures are, in general, closely related to surface temperature, except over the ITCZ regions, where medium and high altitude clouds cover large portions (>65%) of these latitude zones. The reflectivities have a local maximum at ITCZ latitudes, because of the increased reflectivity of clouds relative to ocean and land. The maximum scene IR temperatures correspond to minimum UV reflectivities and occur in the subtropical subsidence zones, where cloud amount is a minimum (<35%), with mid and low clouds predominant. The maxima and minima of total scene IR temperature and UV reflectivity move north or south as the seasons change. The hemispheric and global averages suggest 1) each hemisphere is radiatively colder in its winter season and warmer in its summer season, 2) the globe is radiatively warmer in July than in January, 3) both hemispheres (and hence the globe) are radiatively brighter in January than in July in the UV part of the solar spectrum. These observations are based

¹ Tables relating radiance to equivalent blackbody temperature for the 6.7 μm and 11 μm channels of THIR can be found in Hwang (1982).

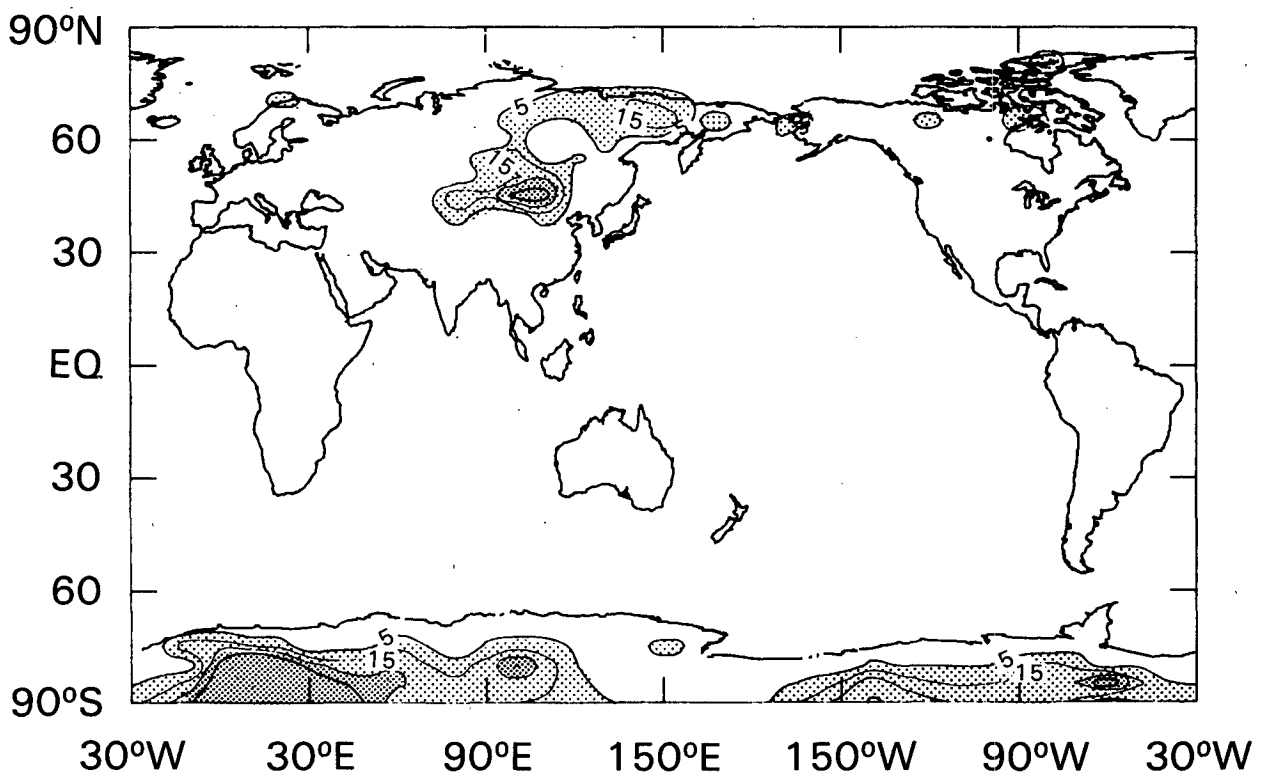
THIR WARM CLOUD

JULY 1979



(a)

THIR WARM CLOUD JANUARY 1980



(b)

FIG. 9. Maps of warm clouds, i.e., clouds whose cloud top radiative temperature is warmer than the surface temperature. These clouds are relatively rare and are associated with atmospheric temperature inversions. The contours show the 5%, 10% and 15%—amount levels for (a) July 1979, and (b) January 1980.

TOTAL SCENE IR RADIATIVE TEMPERATURE (K)

	SH	NH	GLOBE
--- JULY 1979	274	282	278
----- JANUARY 1980	276	273	274

UV REFLECTIVITY

	SH	NH	GLOBE
— JULY 1979	32	33	33
- - - JANUARY 1980	34	34	34

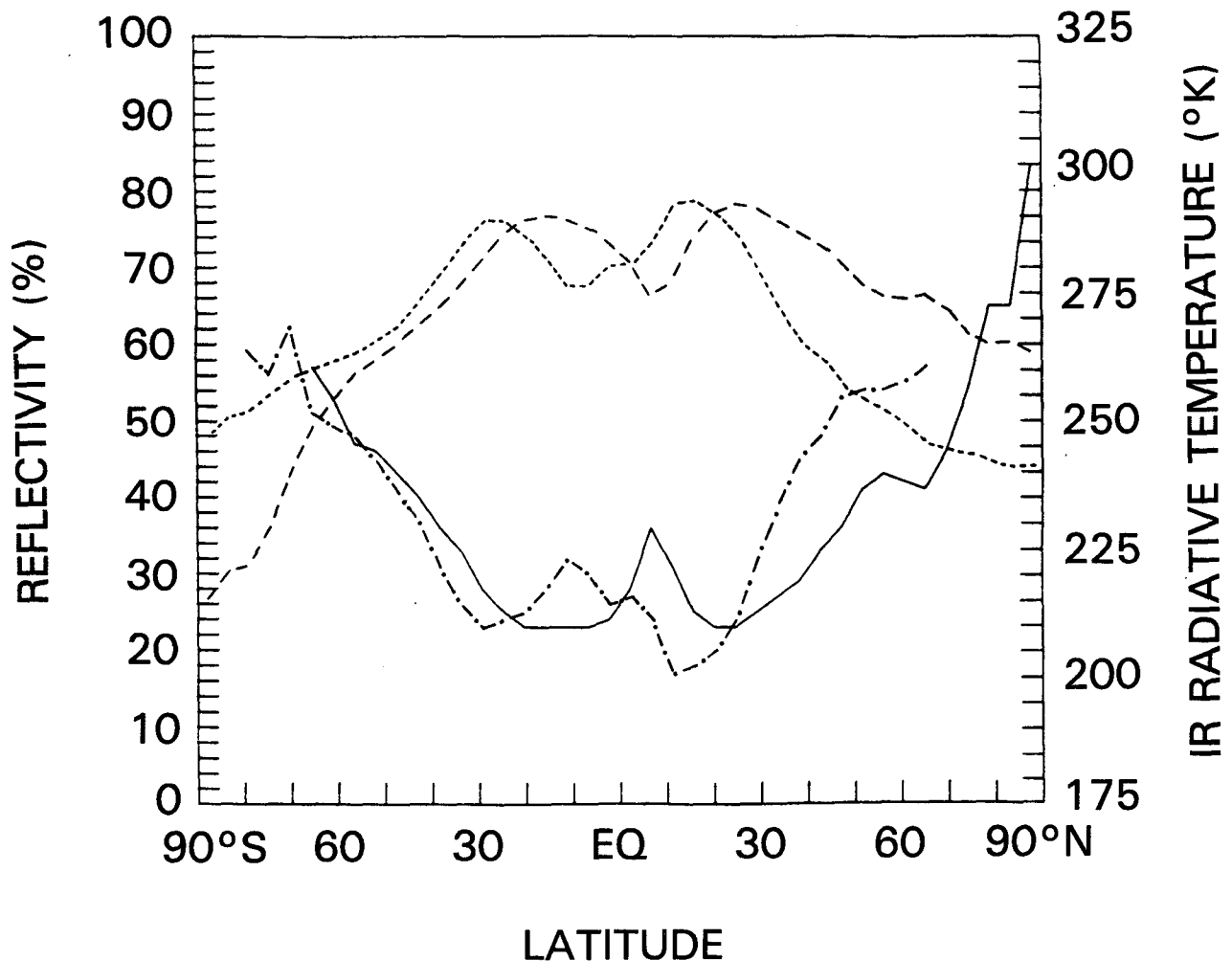


FIG. 10. Zonal averages of total scene IR ($11\ \mu\text{m}$) radiative temperature and TOMS (UV) reflectivity for July 1979 and January 1980.

on narrowband radiation measurements and, therefore, should not be interpreted in terms of the Earth's radiative energy balance. They are presented only to show the consistency of the Nimbus-7 IR and UV radiance data sets.

In Fig. 11a, the clear sky and cloud IR temperatures for different cloud altitudes in July 1979 are plotted as solid lines. The cloud altitude boundary IR threshold

temperatures are plotted as dashed lines. As expected, the clear sky IR temperatures are greatest among the four solid lines in low and midlatitude zones, but become colder than low and midlevel clouds in the Antarctic, where strong temperature inversions occur in Antarctic winter (dark) months. In Fig. 11b, the zonal means of clear sky and cloud IR temperatures and boundaries for different altitudes are plotted for Jan-

NIMBUS-7 ZONAL MEAN OF IR RADIATIVE TEMPERATURES FOR ASCENDING ORBITS 7/79

IR RADIATIVE	SH	NH	GLOBE	BOUNDARY	SH	NH	GLOBE
CLEAR	286	295	290	CLEAR/LOW	277	285	281
LOW	278	282	280	LOW/MID	277	284	281
MID	265	275	270	MID/HIGH	251	259	255
HIGH	232	244	240				

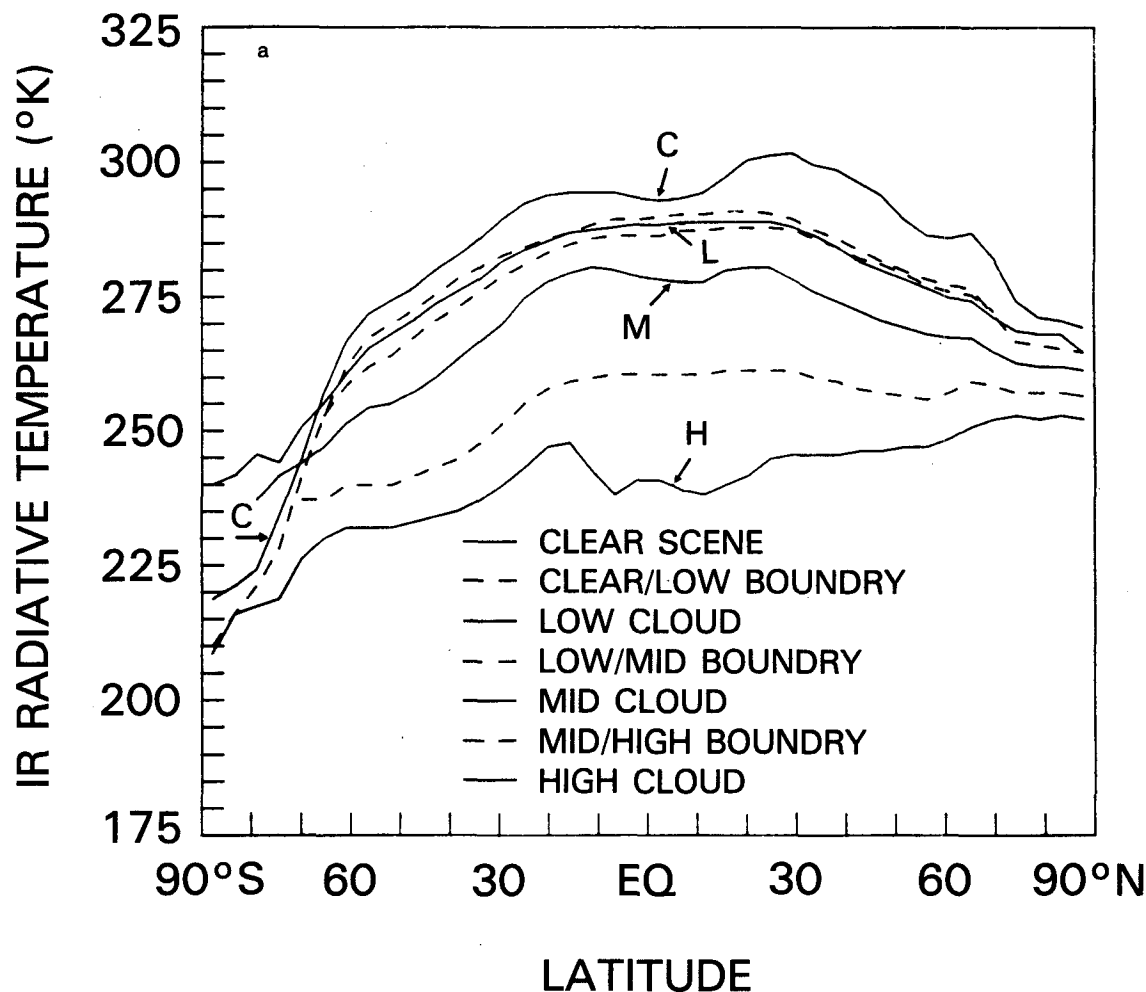


FIG. 11. (a) Zonal averages of cloud IR radiative temperature for different altitude categories (C—clear, L—low, M—middle, H—high) and the cloud altitude classification thresholds for July 1979.

uary 1980. Relationships similar to July 1979 are seen. In general, the zonal averaged cloud IR temperatures fall between respective cloud altitude temperature boundaries. However, in high latitude zones, the low

and mid cloud temperatures do exceed the clear sky temperature. The low clouds temperatures are being sensed by THIR at locations which are warmer than the warm cloud/no cloud threshold used when cli-

NIMBUS-7 ZONAL MEAN OF IR RADIATIVE TEMPERATURES FOR ASCENDING ORBITS 1/80

RADIANCE		SH	NH	GLOBE	BOUNDARY	SH	NH	GLOBE
CLEAR	C	288	284	286	CLEAR/LOW	282	275	279
LOW	L	277	276	277	LOW/MID	279	(—)	(—)
MID	M	270	267	268	MID/HIGH	255	251	253
HIGH	H	241	239	240				

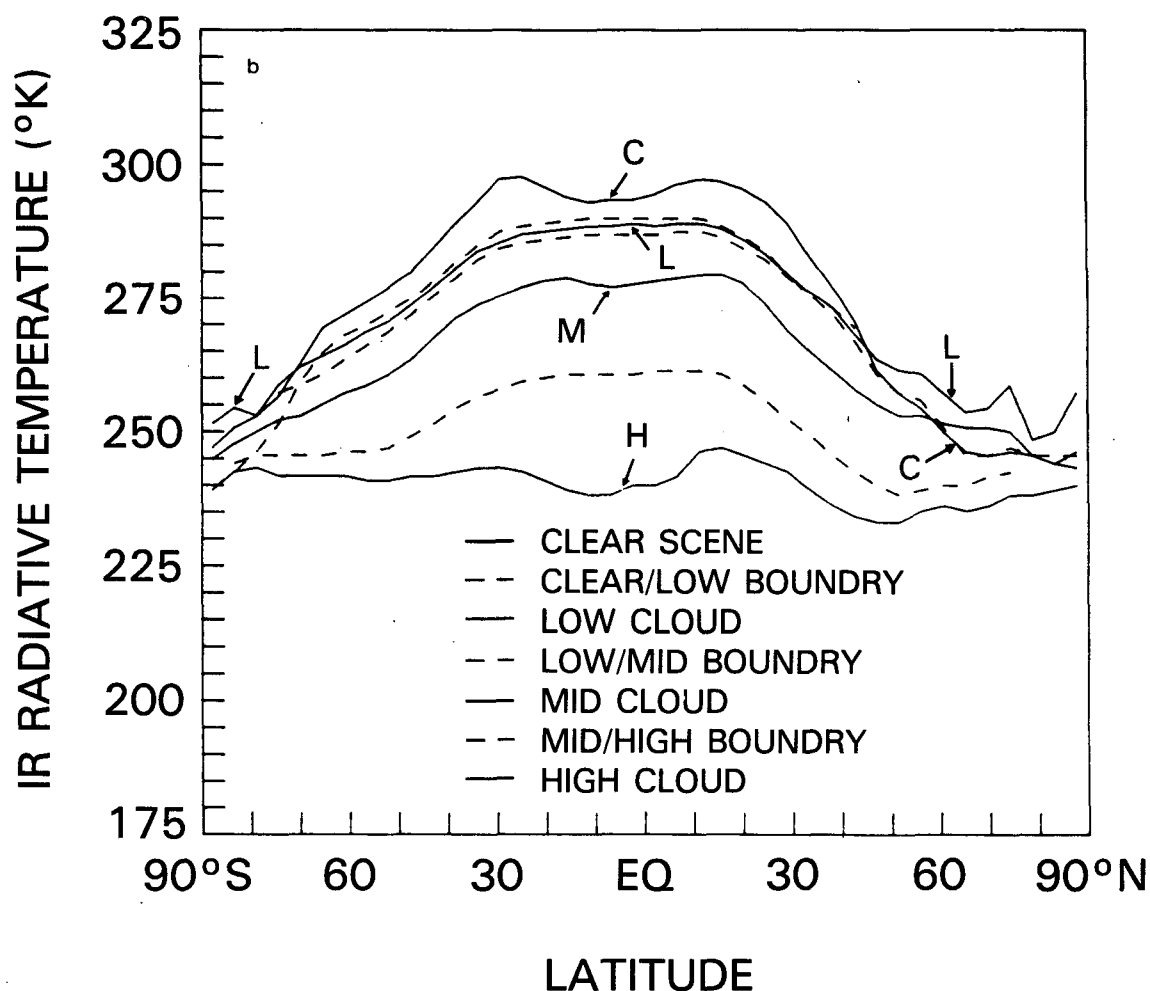


FIG. 11. (b) Same as (a) except for January 1980.

matological inversions occur. Without this provision in the IR algorithm, cloud amount in these regions would be systematically underestimated. Average mid cloud temperatures are greater than the clear sky values only as a consequence of averaging in a zone with

large variations in terrain height or temperature profile. The bispectral algorithm does not allow mid cloud to have a temperature greater than the clear sky value in a target area. Only low cloud can have this property.

The boundary temperatures illustrate the narrow

temperature range allowed for low clouds, which further explains why stratus and stratocumulus clouds are commonly classified as middle clouds. The behavior of the boundaries at the poles is consistent with the logic that is used by the IR algorithm (cf. Stowe et al. 1988), e.g., when temperature inversions or large uncertainties in the clear-sky temperatures occur.

The hemispherical and global average tables shown in Figs. 11a and 11b are for heuristic purposes. The left-hand table shows the mean value of the IR radiative temperature (K) associated with high, middle, and low clouds and clear regions. The associated mean boundary temperatures are shown on the right. Some target areas lack monthly averages for one or more of the quantities. For instance, low/mid boundaries are not recorded when the low/mid boundary is warmer than the clear/low threshold, since it is not used for cloud determination. The absence of an average low/mid boundary radiative temperature for the Northern Hemisphere in January means that the low/mid boundary temperature was recorded for less than 75% of the hemispherical area. Nevertheless, the mean temperature of low and midlevel cloud, which can be observed in the absence of a low/mid boundary (cf. Stowe et al. 1988), appears in the left-hand table. The hemispheric and global averages indicate 1) the clear-sky radiative temperature of the Earth is greatest in July and least in January, with the respective winter hemisphere having lower temperatures than the summer hemisphere, consistent with the scene radiance analysis; 2) this is also observed for the low, mid, and high cloud radiative temperatures; and 3) the extremes in radiative temperature occur in July, where the Northern Hemisphere clear-sky temperature is 295 K and the Southern Hemisphere high cloud temperature is 232 K.

The difference between noon and midnight IR radiances were examined for four different cloudiness categories; clear (0%–5% cloud), partly cloudy (6%–50%), mostly cloudy (51%–95%), and overcast (96%–100%) corresponding to the cloud classification defined for ERBE data processing in Smith et al. (1986). The tropical latitude band of 0°–18°S for the months December 1979 through February 1980 was selected for this analysis. Land and ocean target areas were studied separately. Figure 12 shows the total scene radiance measured by THIR as a function of the four cloud categories for ocean (a) and land (b) areas as determined from the noon bispectral cloud algorithm, the IR-only cloud algorithm at noon, and the IR-only algorithm at midnight. Figures 13a and 13b show the percent population of the ocean and land target areas, respectively, within each cloud category.

Land and ocean regions show distinctly different cloud amount/radiance characteristics. Over land in the southern tropics, the noon radiances are larger than midnight radiances for both clear and cloudy. Further, at noon, the IR algorithm and the bispectral algorithm give very similar results both for radiances (Fig. 12b)

and category percentages (Fig. 13b). Note also, that near midnight, the percentage of overcast areas increases while that of partly and mostly cloudy decreases from near noon values. The explanation for this behavior would appear to be straightforward. The surface temperature of land areas normally increases during the day and then decreases at night, due to the diurnal cycle in solar insolation. Consequently, cloud activity and cloud top altitudes increase from noon through the evening due to related diurnal changes in atmospheric stability. This produces higher (colder) and larger area midnight cloud tops.

Over the ocean, the picture is both different and more difficult to explain. Clear and partly cloudy scenes emit the same radiance at noon and midnight and, contrary to land, mostly cloudy and overcast regions have warmer cloud tops at midnight than at noon. Also, the IR-only algorithm at noon shows closer agreement with the midnight cloud top temperature than does the bispectral algorithm. Further, at noon, the bispectral algorithm shows a lower percentage of overcast and a higher percentage of partly cloudy than does the IR-only algorithm.

The explanation for the characteristics of clear and partly cloudy ocean regions seems straightforward. The sea surface temperature has little diurnal variation; thus clear radiances at noon and at midnight are expected to be, and are observed to be, very similar. Further, warm low clouds are frequently scattered clouds which increase the scene albedo but have little effect on the outgoing longwave radiation. Thus it is reasonable that partly cloudy ocean scenes also have the same radiances at noon and midnight, even though the cloud amount occurs with a different frequency, depending on the algorithm being used. The ability of the TOMS algorithm to detect scattered low clouds over water is apparent in Fig. 13a. Here it is seen that some of the clear targets in the IR-only algorithm have been classified partly cloudy by the bispectral one. This is not the case over land as seen in Fig. 13b. This suggests that partly cloudy IR radiances are more clearly distinct from the surface clear-sky temperature over land, making their detection with the IR-only algorithm more exact, thus minimizing the impact of the TOMS algorithm on the bispectral estimate.

The explanation of the characteristics of the mostly cloudy and overcast targets is based on the behavior of the bispectral algorithm when thin cirrus is present, when it yields a smaller total cloud amount than does the IR-only algorithm. Also, thin cirrus clouds have higher radiative temperatures than thick clouds at the same altitude, due to their lower emissivity (higher transmissivity). It so happens that the greatest amount of thin cirrus in January occurs in the southern tropics, as shown in Fig. 7b. Thus, overcast clouds detected by the bispectral algorithm will consist of a smaller proportion of thin cirrus cloud and partly cloudy will consist of a larger proportion than when they are detected

SCENE RADIANCE VS. CLOUD AMOUNT 0-18S. DEC-FEB

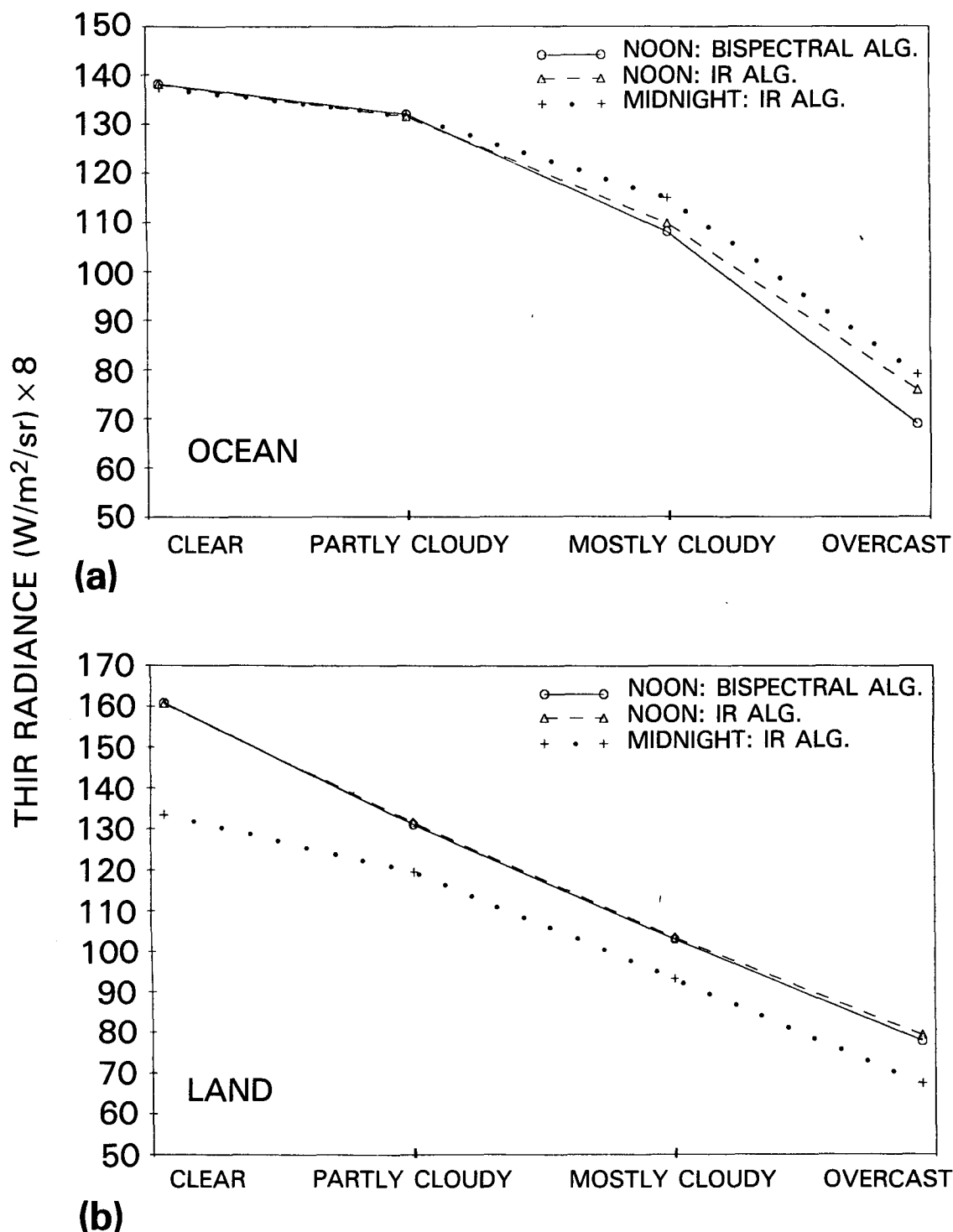


FIG. 12. Total scene radiance measured by THIR as a function of the four ERBE cloud categories (see text) as determined from the bispectral cloud algorithm, the IR-only algorithm at noon and IR-only algorithm at midnight for (a) ocean, and (b) land in the latitude zone 0°–18°S during December 1979 through February 1980.

SCENE POPULATION (%) VS. CLOUD AMOUNT O-18S. DEC-FEB

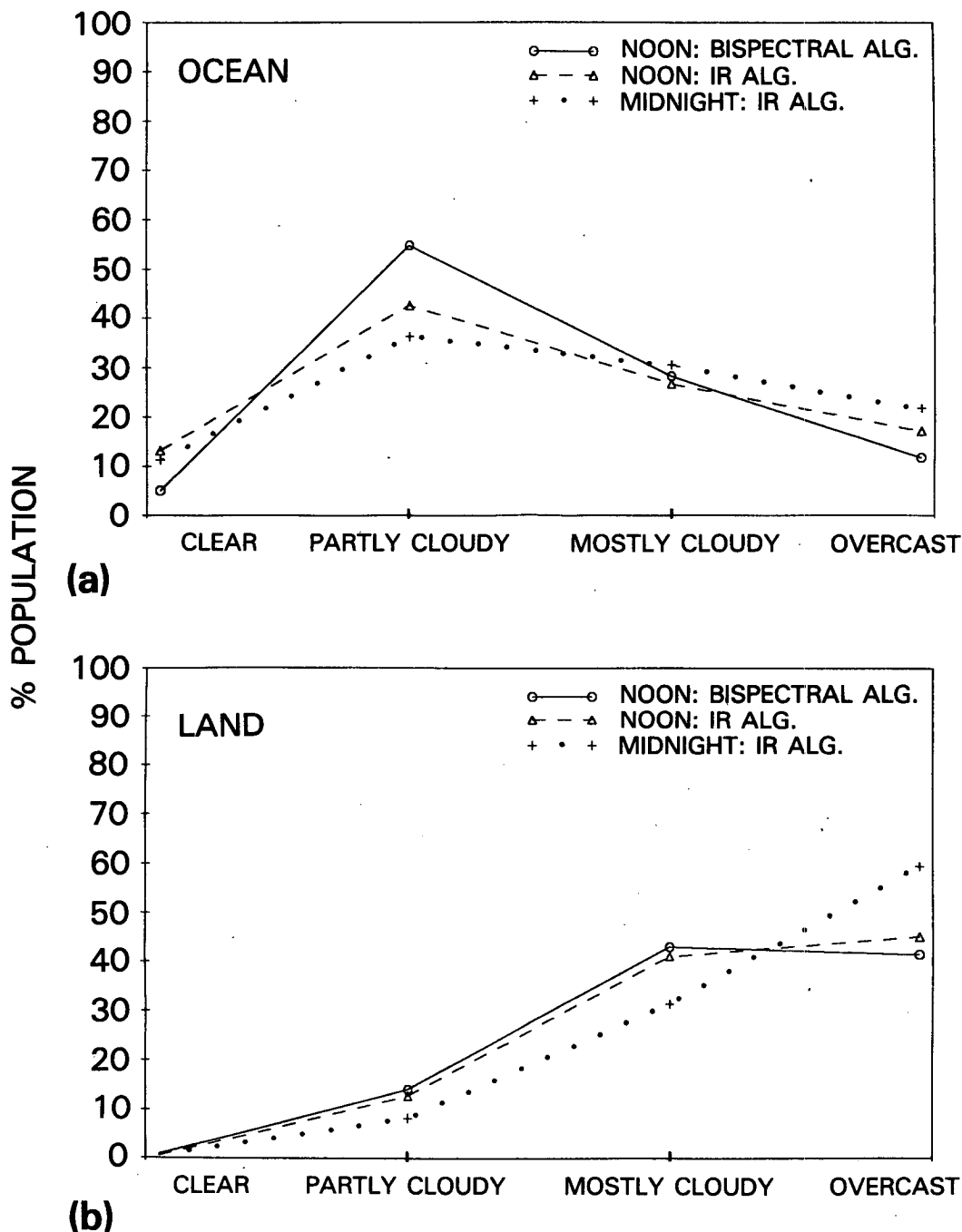


FIG. 13. Same as Fig. 12 except for percent population of target areas in each cloud category.

with the IR-only algorithm. Hence, the bispectral-derived overcast cloud temperature is lower (colder) than the nighttime IR-only-derived temperature, as observed in Fig. 12a. This also explains why the bispectral algorithm detects more partly cloudy and less overcast

areas than does the IR-only algorithm, as seen in Fig. 13a.

Based on the above discussion, the differences between the noon and midnight IR-only results in Fig. 12a suggests that the proportion of cirrus in mostly

cloudy and overcast targets is greater at midnight than at noon. Additionally, the results in Fig. 13a suggest that these clouds are more spatially extensive at midnight than at noon, possibly indicating that a diurnal cycle in cirrus producing convective clouds exists over the tropical oceans. The results and interpretations should not, without further study, be generalized to other seasons and other regions.

3. Comparison with other cloud climatologies

a. Zonally averaged total cloud amount

Figures 14a–d show comparisons for 4 months between zonal mean cloud amount estimates from Nimbus-7 and two frequently referenced cloud climatologies, London (1957) and Berlyand and Strokina (BS, 1980a,b), and the cloud climatology for 1979 from the Air Force 3D-Nephanalysis (3DN, compiled by Hughes and Henderson-Sellers 1985; see also Henderson-Sellers and Hughes, 1985). It is noted that the times and types of observations constituting these data sets differ substantially. London (1957), used more than 10 years of Northern Hemisphere surface observations taken at 1200 UTC, and averaged them seasonally. Southern Hemisphere values have been estimated by assuming them to be Northern Hemisphere values in the opposite (half-year) season, an approach used in climate modeling (Gordon 1984). Berlyand and Strokina (BS 1980) used daytime surface observations over a 30-year period and computed a monthly average cloud climatology. The observations were primarily taken from surface synoptic reports, although some satellite observations were included in the later years (Hughes 1984). The Air Force 3DN, which uses surface, aircraft and satellite cloud observations, has been averaged for monthly means by Hughes and Henderson-Sellers (1985) from four observation times per day—0000, 0600, 1200, and 1800 LST.

The Nimbus-7 estimates are shown by three line plots: heavy-solid for daytime (ascending half orbits) using the bispectral algorithm, thin-solid for daytime using the IR-only algorithm without TOMS, and the thin-dashed line representing the nighttime (descending half orbits) algorithm (IR, without TOMS by default except when the poles are illuminated). As there are only relatively small differences in the zonal characteristics among the three Nimbus-7 cloud estimates, their regional differences having been discussed in section 2a, we shall use the bispectral algorithm results to represent the Nimbus-7 climatology. Besides, since all but the 3DN estimates are daytime only, we shall discuss the general characteristics of zonal cloud cover from the bispectral algorithm when comparing it with other climatologies.

Except for the polar regions, all of the climatologies are in relatively good agreement as to the location of the latitudes of maximum and minimum cloudiness. It is noted that differences between the tropical maximum, associated with the ITCZ, and the two subtropical minima, associated with Hadley circulation sub-

sidence, are greater in both single month climatologies than for the two multiyear climatologies. This may be because of differences in time averaging; the longer time averages are smoothed by interannual variability, while the single year results are not. However, it is also likely that since the multiyear data sets are based on surface data primarily, the cause might be from the combination of a lack of observations around this tropical belt, and the difficulty the surface observer has in identifying cirrus cloud and estimating its amount (Hahn et al. 1984). Warren and Thompson (1983) concluded that reconciliation of radiation calculations with satellite observations requires average cloud altitude, emissivity or amount to be considerably higher than they had assumed. They used London's (1957) cloud climatology in their study, which suggests that, had they used the Nimbus-7 estimates, better agreement between calculation and observation would have resulted.

The daytime Nimbus-7 bispectral estimates show that the position of the ITCZ moves seasonally from just north of the equator in April, to about 7°N in July, staying at 7°N in October, and moving into the Southern Hemisphere in January, to about 11°S, when it is also broadest in latitudinal extent. The peak cloud cover in the ITCZ is maximum in July (74%) and minimum in April (63%). The subtropical minima move with the ITCZ peak, the Northern Hemisphere minimum being less than the Southern Hemisphere minimum except in July. The other climatologies, particularly the Air Force, show these same variations with season. Interestingly, the Air Force estimates show the ITCZ to have a double peak in October 1979. The Nimbus-7 results suggest a double peaked ITCZ in January of 1980. The reason that the two single year climatologies disagree on the presence of a double peaked ITCZ in October is not clear. Comparing the January 1980 Nimbus-7 to the January 1979 3DN, there is a considerable difference, approximately 10%–15% in the subtropical minima located at about 15°N and 30°S. Since the observations are for different years, it is uncertain whether the differences in cloud amount are due to interannual variability or to differences in input data and algorithms. In general, the 3DN results are in closer agreement with the Nimbus-7 nighttime results. Since the IR-only algorithms are similar and use common surface temperature data, one might suspect that the reflectance data in the 3DN algorithms yields more cloud than the TOMS algorithm in the Nimbus-7 data, particularly in the subtropical subsidence zones. However, Hughes and Henderson-Sellers (1985) comment on the apparent lack of use of the reflectance data in 3DN. Thus, there must be some other explanation for the generally larger estimates of cloud amount by 3DN relative to Nimbus-7. Perhaps, the explanation lies in the use of surface observations by the 3DN algorithm.

In the Northern Hemisphere extratropics, the Nimbus-7 results, except for July, show cloud amount in-

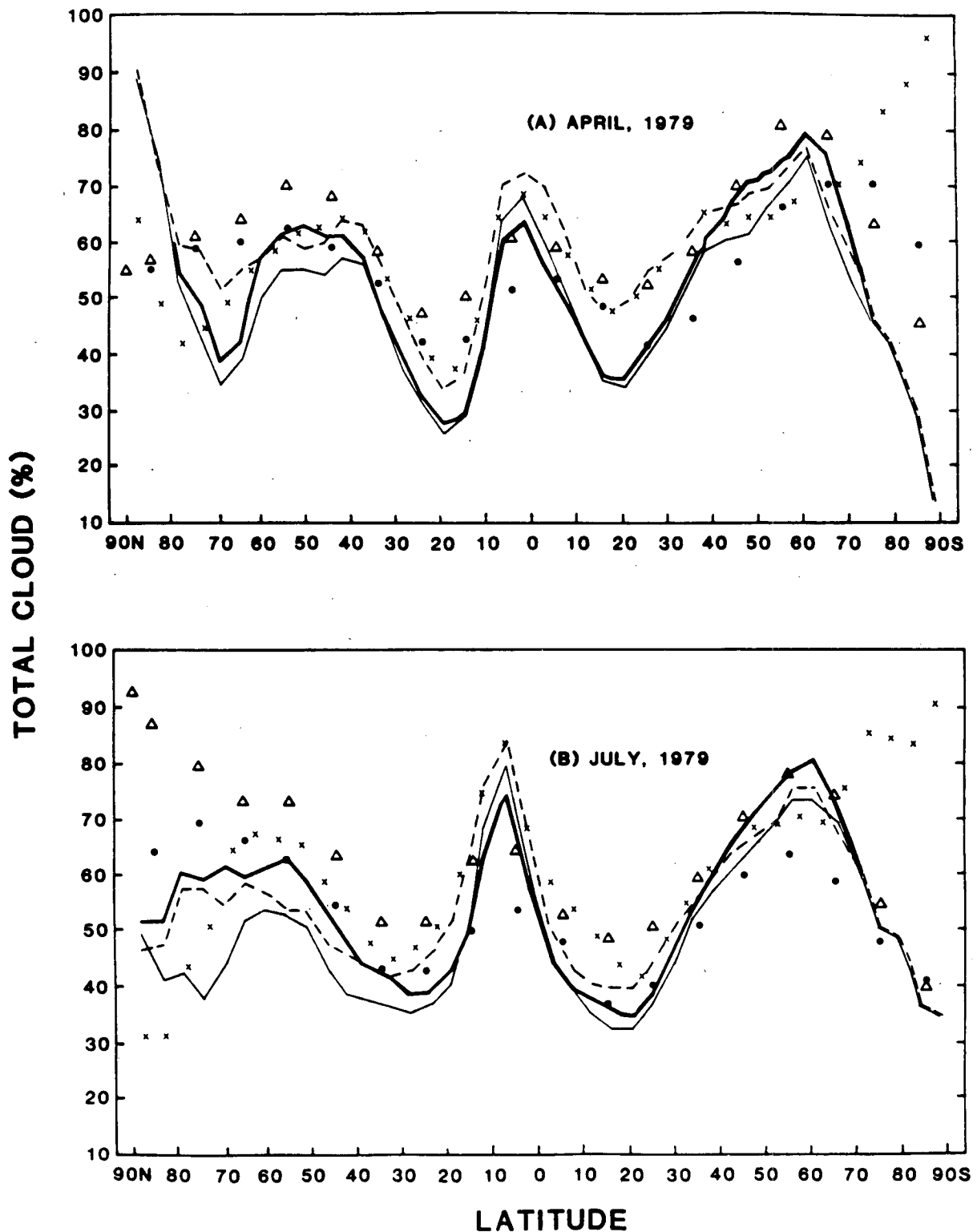


FIG. 14. Zonal averaged total cloud amount for the monthly means of (a) April, (b) July, (c) October, and (d) January. The Nimbus-7 cloud data are shown by a heavy solid line for ascending node (local noon) with TOMS data, a thin solid line for ascending node without TOMS data, and a dashed line for descending node (local midnight). Also shown in the figure are Berlyand and Strokina's (1980) 30 year cloud climatology (Δ); the Air Force 3D-Nephanalysis cloud data for 1979 (\times , compiled by Hughes and Henderson-Sellers, 1985); and London's (1957) multiyear averaged (Northern Hemisphere) cloud climatologies (\cdot). Note that London's SH cloud amount is taken from the value in the NH for the opposite season.

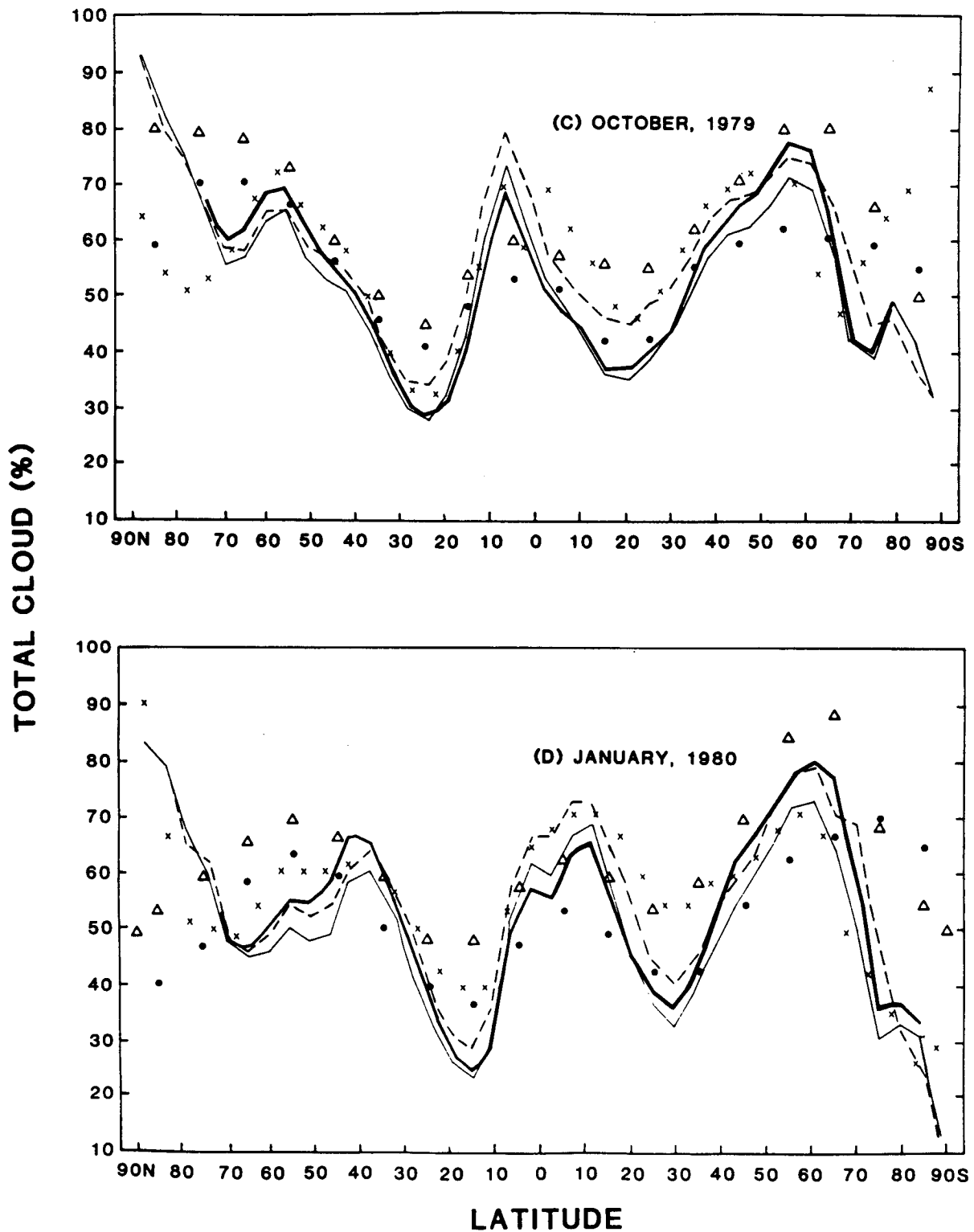


FIG. 14. (Continued)

creasing with latitude, then decreasing and increasing again toward the pole. The latitude of the midlatitude maximum is north of 50°N except in January, where

it occurs at about 40°N, probably the result of the southward movement of the clouds associated with the southerly advance of polar frontal systems during the

Northern Hemisphere winter. The 3DN data set also shows the same characteristic. However, northward of about 60°N, there is no clear agreement between any of the climatologies, except that the 3DN has more of the characteristics of the Nimbus-7 than either of the others.

There is some evidence that the recent multiyear compilation of Beryland and Strokina (1980a,b) is probably the most accurate estimate in the polar regions. Vowinckel and Orvig (1970), using some data sources which overlap with Beryland and Strokina, report considerably more Arctic cloud amount in July than in January. Most of the July increase in cloudiness is due to low relatively thin stratus clouds. The physics of the formation of summer clouds over the Arctic Ocean is also discussed by Herman and Goody (1976) and Curry and Herman (1985). They note that the atmospheric moisture content is small during the polar winters and this is also true during the summer over the south polar cap (see also Nakamura and Oort 1988). Polar clouds tend to be thinner and particle sizes smaller than clouds at lower latitudes. Curry and Herman (1985) report a comparison of a hand analysis of visible and infrared defense meteorological satellite images with the 3DN cloud estimate, from approximately the same data, for the Beaufort Sea region of the Arctic Basin during June 1980. The analyst estimated 71.9% cloud-cover versus 34% for the 3DN. The most important difference was the analyst's estimate of 51.6% low cloud amount over pack ice versus a 21.7% 3DN estimate. There is considerable pack ice throughout the Arctic Ocean during the summer and this forces both the Nimbus-7 and the 3DN algorithms to rely chiefly on the IR cloud estimates, which are often inaccurate for low clouds. Surface observations are fewer and less reliable during the Arctic night, but if we assume that the BS tabulations are also correct during the Arctic winter, it follows that the Nimbus-7 overestimates the Arctic cloud amounts in October, January and April. Since the Nimbus-7 estimates only a few of these clouds to be low clouds, this further implies that the observed THIR IR radiative temperatures are lower than the clear scene radiative temperatures predicted from the 3DN Air Force surface temperatures. In general, the 3DN Air Force Arctic temperatures were found to agree well with reported NOAA temperature fields (Stowe et al. 1988), but these results suggest that further investigation may be necessary. In the polar regions, the surface is often covered by snow or ice and in the winter there is normally little thermal contrast between the surface and even high clouds. Satellite retrieval of polar cloud amount is therefore a difficult art that requires further study.

In the Southern Hemisphere extratropics, the Nimbus-7 results show that cloud amount increases and then decreases with increasing latitude, as it does in the Northern Hemisphere. Over Antarctica, however, the cloudiness continues to decrease, rather than increase as is typical in the Northern Hemisphere. In-

terestingly, the peak midlatitude cloud cover in the Southern Hemisphere does not vary greatly with season, having a value between 70% and 80% and being located near 60°S all year long. October and January hint at a secondary maximum on the Antarctic continent, but the Nimbus-7 cloud-cover data over Antarctica are unreliable due to the difficulty of identifying cloud over snow and ice-covered surfaces and where temperature lapse rates are small. In addition, the Air Force surface temperature analysis, on which the current threshold method is largely based, systematically overestimates surface temperatures over Antarctica by up to 40°C compared to surface station reports. As a result, climatological surface temperatures have been used in that region in the Nimbus-7 cloud algorithm.

The effects of erroneous Air Force temperatures used in the 3DN algorithm to determine the infrared cloud/no cloud threshold, are evident in the 3DN results for the Antarctic for most months starting with April 1979. The elevated surface temperatures used explain why the 3DN estimates of cloudiness are so much larger than the other estimates over Antarctica except during January. Hughes and Henderson-Sellers (1985) state that the 1979 3DN cloud cover estimates for Antarctica are unreliable. The use of climatological surface temperatures by the Nimbus-7 sharply reduces cloud amount estimates compared to the 3DN. However, only in July 1979 was there good agreement with the multiyear results of BS. The Nimbus-7 estimates show considerably more cloudiness in July than in January, while Beryland and Strokina indicate slightly more cloudiness in January than in July. Warren et al. (1986) agree with BS on this point.

A comparison between hemispheric and globally averaged cloud amounts estimated by these climatologies is given in Table 1. Several interesting features are apparent: excluding London's Northern Hemisphere-only climatology, all climatologies agree that, except for July, the Southern Hemisphere is more cloudy than the Northern Hemisphere; the maximum hemispheric cloud cover occurs in the summer season and the minimum in the winter season. Among those daytime cloud climatologies, BS has the largest estimate of global annual average amount, 60%, with London and Nimbus-7 (local noon) having the smallest estimates of 51%. The Air Force 3DN globally and diurnally averaged value is 57%. If the Nimbus-7 nighttime estimate is included in the global average, the Nimbus-7 estimate increases to a value of about 54%, closer to the 3DN estimate.

The differences between the three Nimbus-7 estimates shown zonally averaged in Figs. 14a–d, have been discussed in section 2a, using regional maps (Figs. 1a, b and 2a, b). An additional characteristic which is apparent from the zonal plots, is the IR algorithm total cloud amount is greater than the bispectral algorithm total cloud in the intertropical convergence zone (ITCZ) peak region, confirming that this is a region with large amounts of cirrus cloud. On the con-

TABLE 1. Hemisphere and global averages in percent of total cloud amount for the four months representing four seasons, separately, and annually averaged.

Month	January			April			July			October			Four season average		
Climatology	N.H.	S.H.	Global	N.H.	S.H.	Global	N.H.	S.H.	Global	N.H.	S.H.	Global	N.H.	S.H.	Global
N-7 Day	47	55	51	49	53	51	52	51	52	51	51	51	50	52	51
N-7 Day (w/o TOMS)	45	53	49	47	51	49	48	49	49	51	50	50	48	51	49
N-7 Night	50	60	55	55	60	57	56	53	54	55	57	56	54	58	56
London (10 years)	48	52	50	51	53	52	52	48	50	53	51	52	51	51	51
BS (30 years)	57	65	61	58	62	60	62	59	60	59	63	61	59	62	60
AF 3DN 1979	53	61	57	54	60	57	59	58	59	53	60	56	55	60	57

trary, the bispectral total cloud is greater than the infrared algorithm cloud amount in the extratropical areas, consistent with the fact that low cloud is not being as efficiently detected by the IR-only algorithm.

For July 1979, Fig. 14b shows that over 15% cloudiness is added by TOMS to the daytime IR estimate in the North Polar latitudes. In comparison with the IR nighttime estimates, it appears that either the daytime algorithm is in error or that there is a large diurnal change in cloud cover. Actually, the nighttime estimate at this latitude is a bispectral product, since solar illumination is present on the descending part of the orbit. Thus, the diurnal behavior of the cloud cover in polar summer is better represented by comparison of the bispectral daytime estimate with the nighttime estimate.

A preliminary version of the ISCCP C1 cloud data set has been distributed to interested scientists for study and comment. It uses the cloud algorithm described in Rossow et al. (1985). It is expected that the final ISCCP cloud algorithm will yield cloud estimates similar to, but slightly smaller than, those from the preliminary version (Rossow, personal communication). Several studies comparing the Nimbus-7 cloud data set with this version of the ISCCP cloud data set have been initiated.

Professor Robert Cess, State University of New York at Stony Brook, kindly furnished the plot of zonally averaged, local noon cloud amount for July 1983, shown in Fig. 15. The thin, upper solid line indicates the ISCCP total cloud estimate, the thick, lower solid line is the Nimbus-7 cloud estimate, and the dashed line shows a modified ISCCP estimate. This latter estimate results from doubling the magnitude of the visible and infrared cloud/no-cloud (c/nc) ISCCP thresholds, a magnitude change consistent with the expected uncertainties of these thresholds (Rossow, personal communication). In general, all three curves identify the same equatorial belt of maximum cloud cover with relatively clear subtropical subsidence regions on either side followed by midlatitude cloud maxima, but there are notable differences between the three curves. For example, from the equator to 10°N

latitude, ISCCP estimates a zonal average 72% versus 62% for Nimbus-7 (a ratio of 1.16), while between 10°S and 20°S latitude, the ratio of cloud estimates is 1.47. The ISCCP algorithm estimates a mean global cloud cover of 66% versus a Nimbus-7 estimate of 51%.² The modified ISCCP algorithm (dashed line), is in much better agreement with the Nimbus-7 cloud estimate, the global mean being reduced to 52%. However, there are still some significant differences with Nimbus estimates, particularly in the southern extratropics. Note that in the tropical cloud belt, the modified ISCCP estimate is now lower than the Nimbus-7 estimate. The regions most greatly affected by doubling the ISCCP thresholds are those where low altitude marine stratus clouds are prevalent (Rossow, personal communication).

The Nimbus-7 cloud data set starts in April 1979 and continues for 6 years, while the ISCCP data set starts in July 1983 and is expected to continue at least until June 1990. If these two data sets can be combined, after removal of systematic differences, a cloud climatology of over 11 years would exist for weather and climate study. A objective of the study, initiated at NOAA/NESDIS, is to understand the causes of differences between the Nimbus-7 and ISCCP cloud estimates and of determining ways of adjusting the ISCCP cloud estimates to more closely agree with the Nimbus-7 estimates. Comparisons of ISCCP cloud estimates computed for (165 km)² areas at 1200 UTC from METEOSAT data, with Nimbus-7 local noon estimates at the same locations for several days in July 1983 have been conducted. These results have led to some preliminary conclusions.

A principal cause of the systematic difference between the two cloud estimates appears to be the difference between the respective bispectral algorithms, where cloud amount estimates from the reflected solar and emitted thermal channels are merged into one estimate. Nimbus-7 estimates area cloud averages sepa-

² Professor Cess used a preliminary version of the Nimbus-7 cloud data tapes. The final version gives a value of 49%.

ZONALLY AVERAGED CLOUD AMOUNT JULY 1983 (12:00)

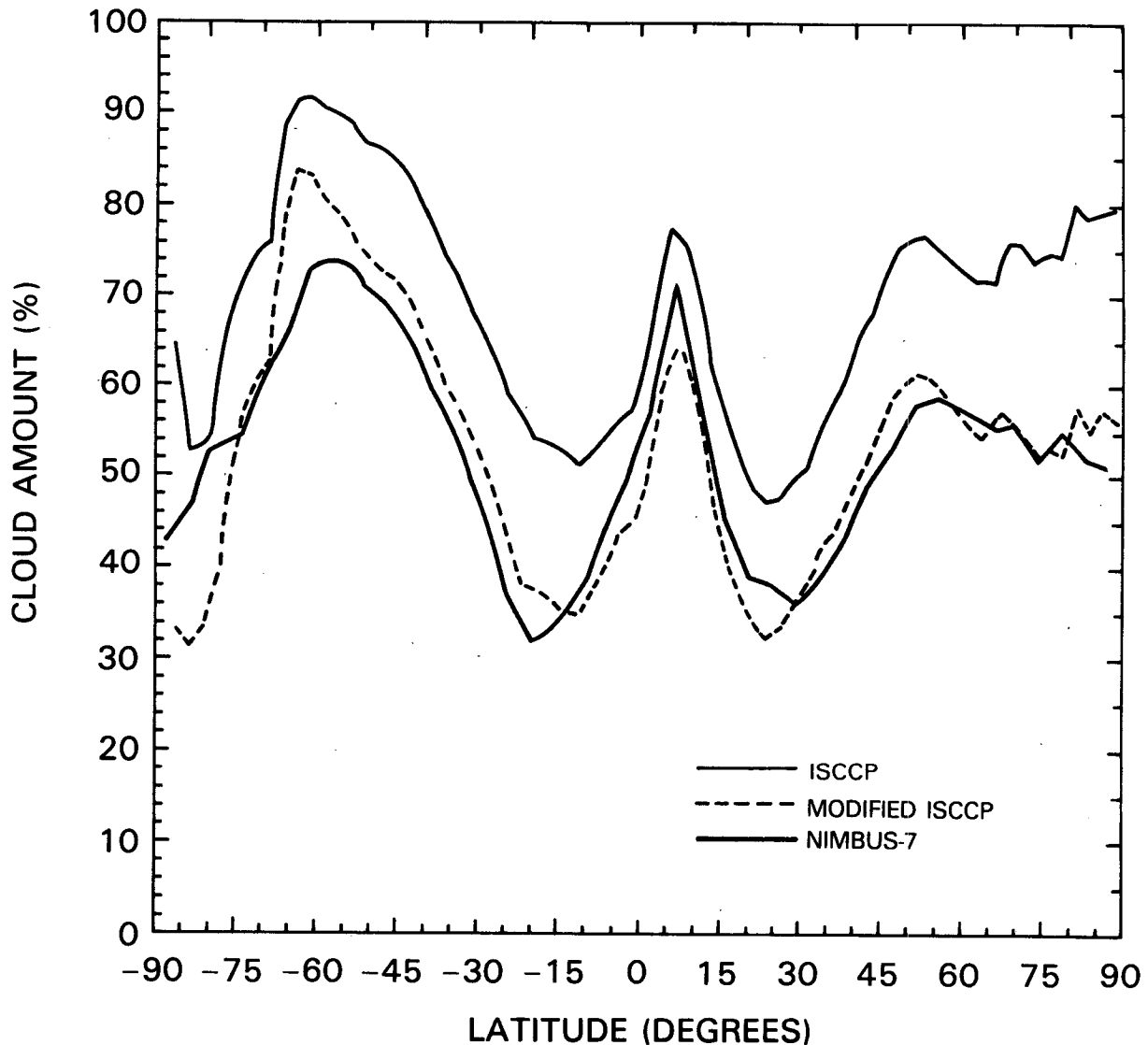


FIG. 15. Zonally averaged total daytime cloud amounts at noon local time for July 1983. Estimates by the Nimbus-7 algorithm (thick, lower solid line) and the preliminary ISCCP algorithm (Rossow et al. 1985) are shown together with a modified ISCCP estimate (see text). This figure is based on information kindly furnished by Professor Robert Cess, State University of New York at Stony Brook (south latitudes are negative).

rately; one from a pixel-counting threshold algorithm applied to the THIR infrared radiances, and the other from a linear-scaling algorithm applied to TOMS UV reflectivities. These separate estimates are then combined into a weighted average estimate for the area. The weight is proportional to IR cloud amount, which is related to cloud altitude (Stowe et al. 1988). The effect is that when the IR is least sensitive to clouds (e.g., when they are low in altitude (small in amount)), the reflectance estimate gets the greatest weight, and conversely, when the IR is most sensitive (e.g., when the clouds are at middle and high altitudes (large in

amount)), the IR estimate gets the most weight. ISCCP, however, uses a pixel-counting threshold algorithm, where the cloud/no-cloud decision for each pixel is based on logic which combines the VIS and IR radiances, rather than separate them. In other words, for a pixel to be considered clear, both the reflected and IR algorithms must agree that it is clear, otherwise the pixel is considered cloud-covered. Conceptually, this would lead to systematically larger ISCCP estimates of cloud cover than would be estimated with the Nimbus-7 approach. As an example, suppose all of the METEOSAT pixels were distributed equally among the

four possible VIS/IR cloud/no-cloud combinations (i.e., each combination accounted for 25% of the total number of pixels for an area). Then the ISCCP bispectral algorithm would estimate 75% cloud cover. The Nimbus-7 bispectral algorithm applied to the same pixel data, would yield an estimate of 50%; since the VIS and IR algorithms separately would estimate 50%, and each would get a weight of 50%.

Other possible causes of differences are:

- 1) The ISCCP algorithm implicitly allows for the uncertainty in defining the c/nc thresholds and for the effects of partially filled fields of view, while the Nimbus-7 algorithm treats these explicitly. As a result, the Nimbus-7 IR c/nc threshold is, on the average, 3 K lower over oceans than that used by ISCCP. This is totally consistent with the lowering of cloud amount that Cess observed in modifying the ISCCP algorithm by doubling the c/nc thresholds (which amounts to lowering the ISCCP IR threshold over oceans by 3 K). Coakley (1987) concluded that a c/nc threshold closer to the Nimbus-7 value was needed to agree with results from the spatial covariance technique (Coakley and Bretherton 1982).

- 2) ISCCP undersamples the area fully sampled by Nimbus-7, by about 1 part in 36 for METEOSAT data (1 part in 16 for GOES data), i.e., only 3% (6%) of an area is sampled in estimating the average amount of cloud in it (this is done to reduce the radiance data volume). Seze and Rossow (1989), have concluded that one has to spatially average instantaneous estimates over approximately $(500 \text{ km})^2$ areas or temporally average $(250 \text{ km})^2$ estimates over about a 10-day period in order to remove undersampling errors.

- 3) Nimbus-7 uses shelter temperature over land to estimate the IR c/nc threshold, while ISCCP uses skin temperature, making ISCCP more sensitive to thin high clouds over land areas.

- 4) ISCCP uses visible radiation while Nimbus-7 uses UV radiation to estimate cloud amount from reflected sunlight. This makes the determination of the ISCCP reflectance c/nc threshold a complex, time series analysis process, sensitive to errors from cloud contamination in geographical regions where clouds are persistent. A constant value can be used for the Nimbus-7 c/nc reflectance threshold, since, in the UV, land and ocean surfaces have reflectivities that are within several percent of 8% when cloud-free (Eck et al. 1987). Also, over the oceans, the ISCCP visible radiances cause Saharan dust to be interpreted as water cloud, while in the UV, possibly because the dust is more absorbing there than the visible (d'Almeida 1987), dust clouds are not included in the Nimbus cloud estimates.

- 5) Nimbus-7 uses Air Force surface temperature analysis fields and an empirical correction for water vapor attenuation to estimate the IR c/nc threshold, while ISCCP uses observed radiances identified as clear from a time series analysis of the radiances. In regions where high humidity or cloud cover persist, the c/nc

thresholds of the two algorithms could be systematically different.

The importance of each of these various algorithm differences undoubtedly varies from one region to another and depends on the type of clouds being observed. Determining the optimum adjustments to the ISCCP algorithms to best match the Nimbus-7 algorithm will require further study. Wisely, the ISCCP data sets have been constructed to facilitate reanalysis, so that making adjustments to the algorithms should not require a massive reprocessing effort.

b. Zonal averaged cloud amount by type

For the purposes of climate modeling and Earth radiation budget analysis, not only is the total cloud amount important, but information on the altitude of the clouds is also needed. A comparison between the high, mid, and low level cloud zonal means from Nimbus-7 and the London (1957) cloud climatologies is shown in Fig. 16 for July 1979, and Fig. 17 for January 1980. There are two important differences between the definition of cloud altitude from Nimbus-7 and that of surface based observations which are used in London's climatology. The first difference is in the definition of the cloud height which, for surface observers, is influenced strongly by cloud base height, while for Nimbus-7, the height is determined from infrared radiances of the cloud tops. Thus, only in the case of a very thin single layer cloud, will these two definitions generally yield the same cloud altitude, while in most other cases the satellite derived cloud height will be greater. The second difference occurs for the case of multilayer clouds where the surface observer will report the base height of the lowest cloud layer while the radiances measured from satellite will be from the top of the highest layer. Thus it is not surprising that the amount of low cloud in London's climatology is greater than the Nimbus-7 low cloud at all latitudes, since the Nimbus-7 only maps low clouds which have no overlying mid or high level clouds. The largest discrepancy, however, occurs for midlevel cloud where the surface observers have reported much less cloud at all latitudes, probably due to a combination of multilayer masking and differences in defining cloud altitude. The latter cause probably explains why London's low cloud amount is most similar to the Nimbus-7 middle cloud amount.

In both Figs. 16 and 17, the peak cloud amounts associated with the ITCZ are shown composed mostly of middle and high altitude clouds. The minimum in cloud amount associated with the subtropical subsidence regions are mostly middle level clouds according to Nimbus-7, even though these are regions known to have predominantly stratocumulus and cellular clouds, conventionally defined as low level clouds. This is an excellent example of where low altitude cloud tops are sufficiently cold to be classified as middle cloud by Nimbus-7. In July, the amount of low cloud decreases

Zonal Average Cloud Cover

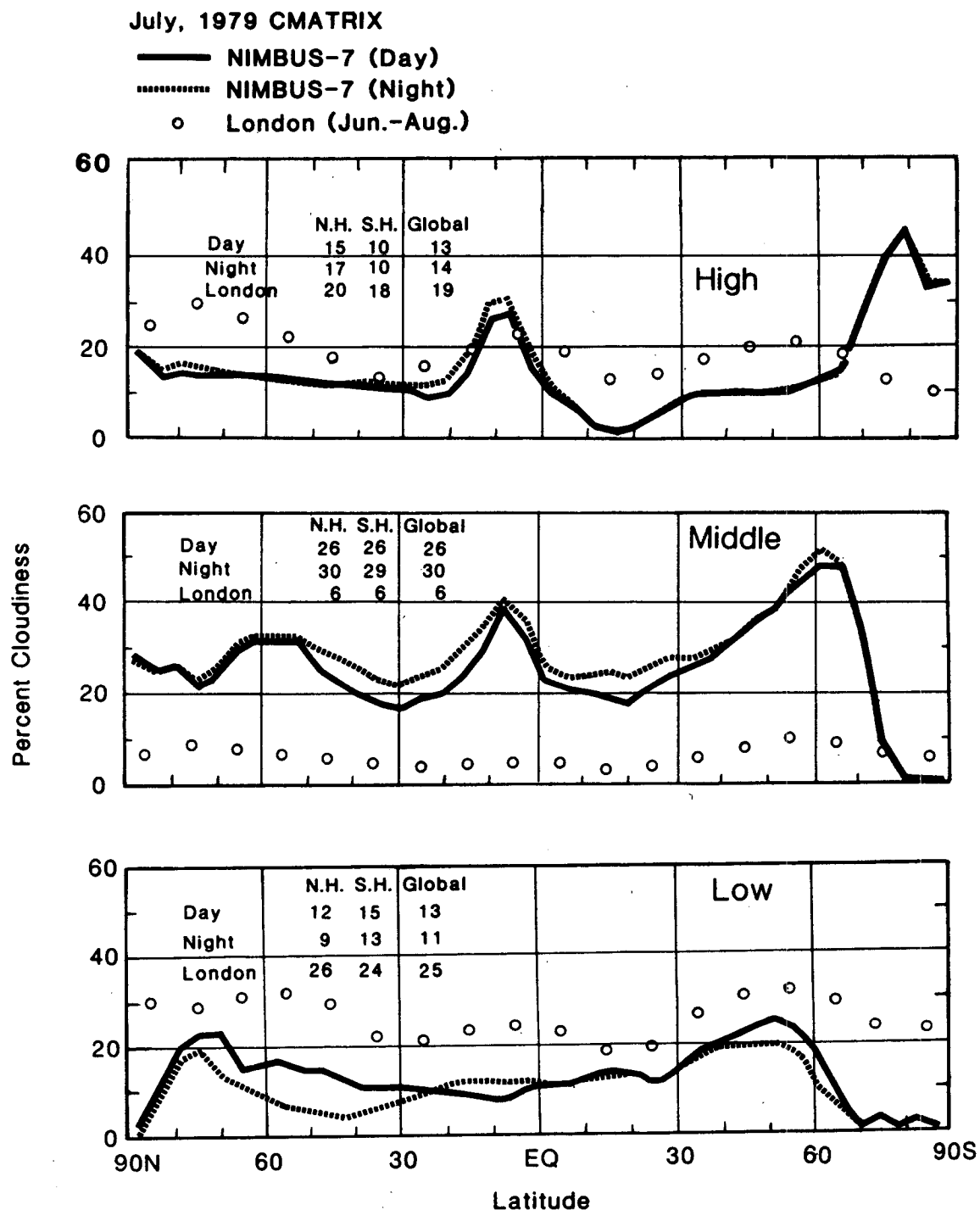


FIG. 16. Nimbus-7 zonal averaged cloud amount of (a) high, (b) middle, and (c) low clouds for July 1979. London's (1957) surface observed cloud climatology for the month of July is also shown. The Nimbus-7 local noon estimates are calculated from the bispectral algorithm, while the local midnight values are from the IR-only algorithm (except at the respective summer poles, where TOMS data have also been used for the descending orbits). Tables of hemispheric and global averages are given for each cloud type within the figure.

Zonal Average Cloud Cover

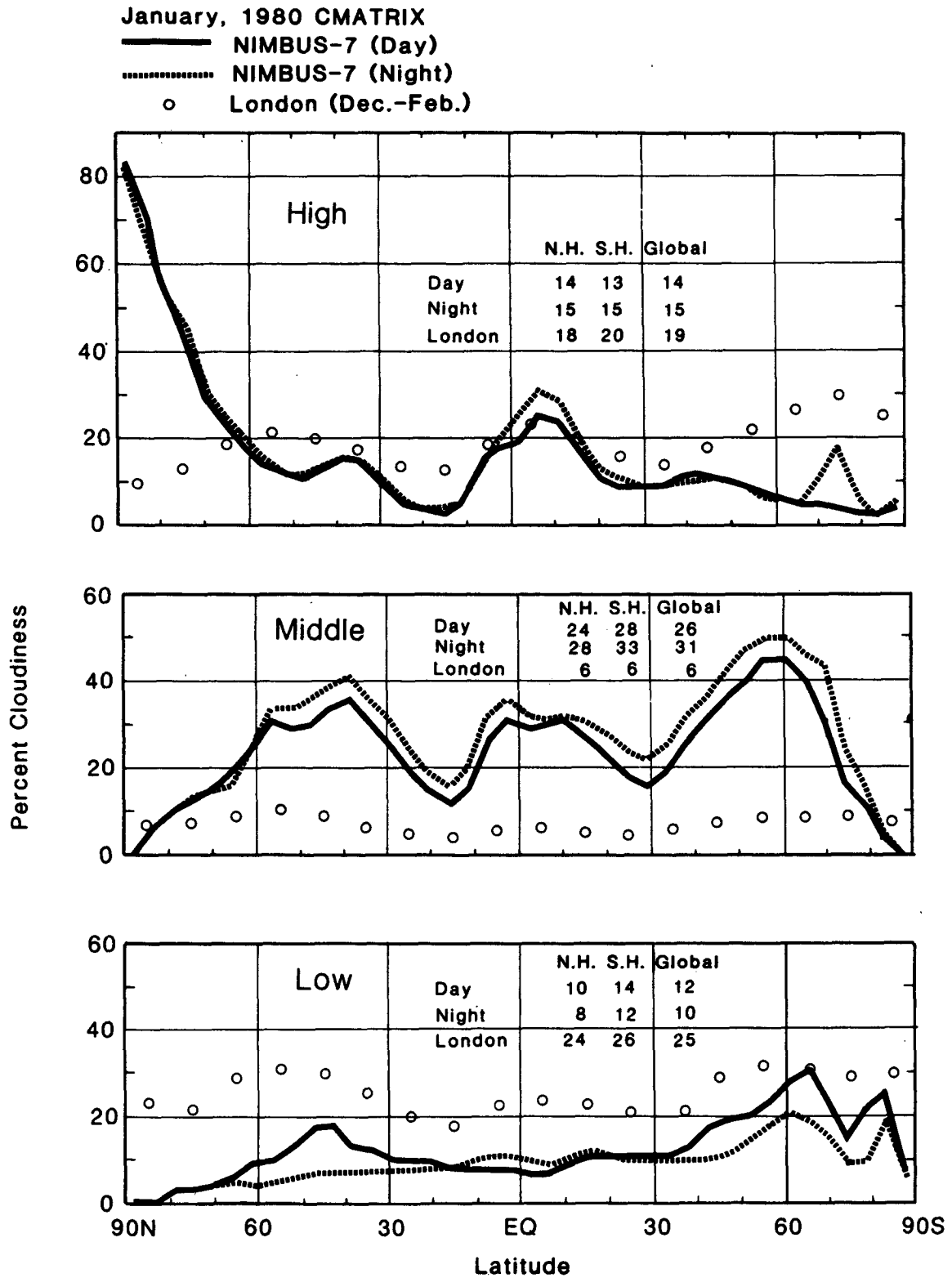


FIG. 17. Same as Fig. 16 but for January 1980.

to zero at the poles, as does middle cloud over Antarctica. For Antarctica, this is the result of the altitude of the continent together with the prevalence of climatological temperature inversions in July, i.e., whenever a cloud is colder than the cold c/nc threshold, it is also characteristically colder than the 4 km mid/high cloud threshold. The north polar reduction in low cloud is more difficult to understand. As was discussed in section 2a, the low cloud in this region would almost all be due to the TOMS algorithm, which for July is operating in both the day and night data (ascending and descending orbit nodes). Its decrease to near zero at the pole suggests that, either low level inversions are climatologically present at the pole, or the Air Force temperature analysis has large spatial variability, both of which would eliminate the possibility for low clouds to be detected by the IR-only algorithm. However, for the TOMS estimate not to have detected low clouds, either the TOMS estimate must have been in very close agreement with the IR-only estimate, or sea ice is being reported by the Air Force analysis, preventing the use of TOMS data.

The middle and high level clouds are more abundant at night than in the day, globally by 4% and 1%, respectively. The low cloud amount shows the effects of the merge algorithm, since the additional amount of clouds detected by TOMS always is assigned to the low cloud amount. For those areas where the total merged NCLE cloud amount is less than the original IR cloud amount, the subtraction of cloud amount is first taken from the low cloud and then middle and high IR clouds, if necessary. The latitudes where the day low cloud amount exceeds the night value corresponds to those latitudes in Fig. 14b where daytime with TOMS exceeds the daytime without TOMS total cloud estimates and vice versa. This is a very important observation as it implies that the amount of low cloud detected by the IR algorithm is about the same, day or night, so that the changes in middle and high cloud are indeed the result of diurnal variability in cloud amount in these regions. That is, the low cloud explains the differences between daytime, with and without TOMS, and the mid and high cloud explains the differences between day and night IR-only estimates. In other words, the low cloud would look essentially the same, day or night, without TOMS.

The interpretations of Fig. 16 are generally applicable to the results shown in Fig. 17 for January 1980. However, there are some interesting differences between the poles in January and July. In January in the Antarctic region, there is less total cloud, which is made up less of high cloud and more of low cloud. The peak in high cloud at about 75°S at night is curious. One possible explanation might be that it is an artifact of surface temperature changes due to variable solar heating explanation might be that it is a result of surface temperature data are used for cloud retrieval in Antarctica and climatological inversions may be present

over this high altitude continent even in January, we speculate that the colder Antarctic surface on the descending orbits is being interpreted as high level cloud, while during the ascending orbits, the surface is warmed sufficiently to be classified as clear. The TOMS is being used both day and night (ascending and descending nodes), for reported snow-free areas, as was the case for the North Pole in July. However, Antarctica is permanently snow-covered, except for northerly coastal areas and some regions which become ice-free in January, so TOMS estimates are rarely available. Obviously, this is a difficult area for satellite cloud retrievals. Other cloud remote sensing techniques and satellite instruments are needed. Perhaps the addition of a 1.6 μm channel to the Advanced Very High Resolution Radiometer (AVHRR) on the NOAA satellites in the 1990s will improve cloud detection over snow covered regions (cf. Warren 1982).

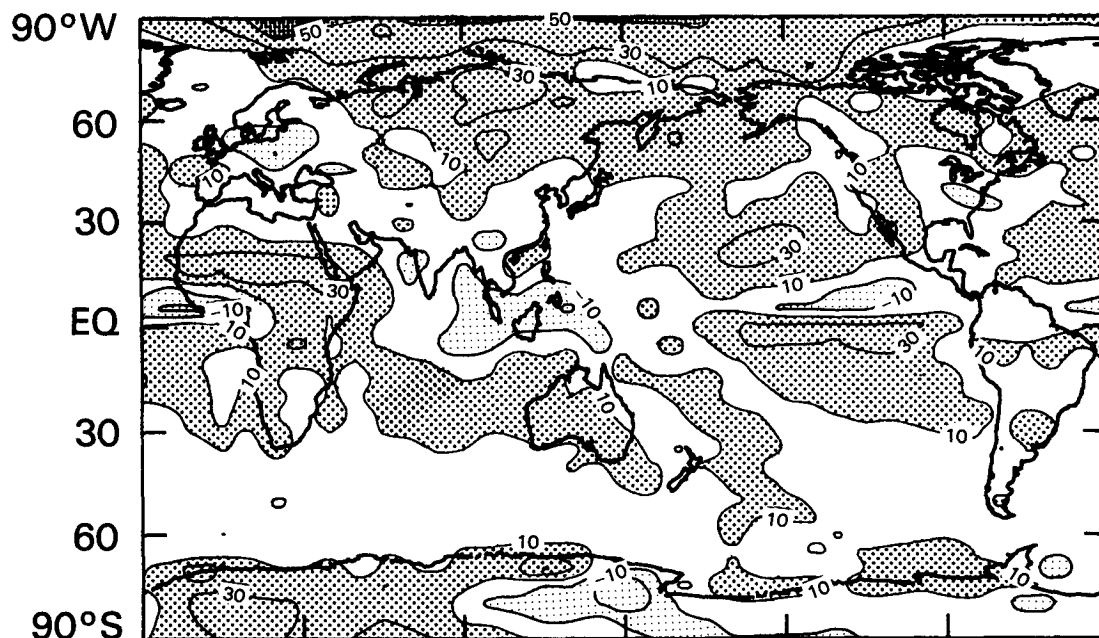
The north polar region, which is in darkness this whole month, shows very little difference day from night. However, high cloud amount is substantially greater toward the pole in January than in July, while middle cloud decreases toward the pole in January, but is rather constant with latitude in July. The fact that there are more clouds in January than in July in the north polar region may be the result of the polar vortex being more intense during the winter period, yielding larger vertical velocities in this region which could produce cloud amount at the high (greater than 4 km) altitude region more effectively than in July. Also, climatological inversions are common in January in the Arctic, and this would make it more difficult for the IR-only algorithm to detect low or midlevel cloud. However, Nimbus-7 estimating more cloud in January than in July, in the Arctic, is contrary to surface observations, as discussed in section 3a.

c. Regional cloud map comparisons

The BS data set, giving monthly mean daytime cloud amount on a 5 deg \times 5 deg lat/long grid are compared to 4.5 deg \times 4.5 deg resolution data of the monthly mean Nimbus-7 cloud amounts. To facilitate comparison between these two data sets, maps of the difference were computed for July and January months (Fig. 18).

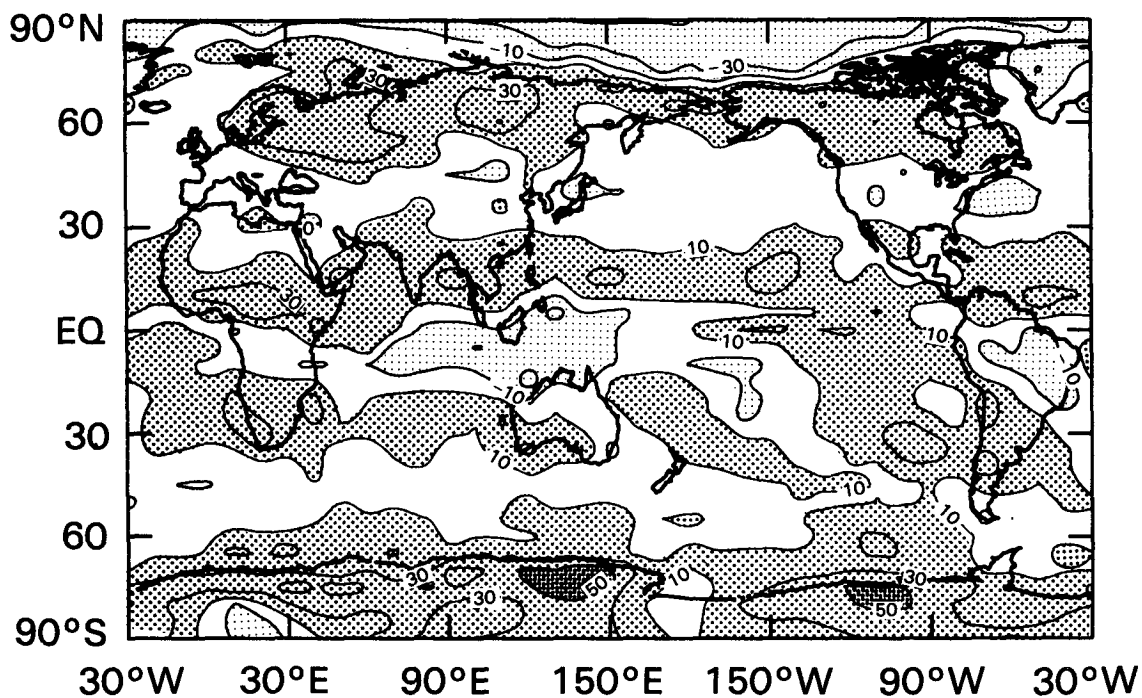
Given that the BS climatology is for a 30-year period and the Nimbus-7 cloud climatology is based on only one month of data, it is expected that there would be some areas with significant differences of total cloud amount. Note also (Table 1) that BS show a global cloud coverage 8% to 10% higher than does the Nimbus-7 data set. Interannual variability in cloud amount can be quite large for many regions, for example, cloudiness perturbations are extensive in El Niño years, and therefore a multiyear climatology is not as likely to have the extreme maxima and minima possible from a single year climatology. Due to this interannual vari-

BERLYAND & STROKINA-NIMBUS-7 JULY 1979



(a)

BERLYAND & STROKINA-NIMBUS-7 JANUARY 1980



(b)

FIG. 18. Maps of the difference between the Beryland and Strokinia (1980) total cloud amount in daytime and the Nimbus-7 total cloud amount from the bispectral algorithm at local noon for (a) July, and (b) January.

ability, it is difficult to interpret the differences between the two data sets since it is not only the input data but also the analysis techniques/algorithms that differ. Therefore, it is not surprising that there is a notable pattern in the differences with the Nimbus-7. For example, Nimbus-7 estimates more cloudiness in the peak ITCZ regions and monsoon regions for all seasons. The polar regions, as already discussed, are also regions with large differences between the two climatologies. The BS cloud amounts are shown to be 10%–30% more than the Nimbus-7 cloudiness for extensive areas at most latitudes, especially in regions of minimum Nimbus-7 cloud amount. For example, the Nimbus-7 July 1979 local minima of the Pacific subtropical high pressure regions are in the range of 10%–40% lower than the BS results. Hughes and Henderson-Sellers (1985), comparing the 3DN of 1979 with BS, also found that the 3DN detects more cloud in the ITCZ and the monsoon regions but less cloud in other areas.

4. Conclusions

The Nimbus-7 global cloud climatology data set provides information on cloud altitude distributions, cloud amounts (twice daily near local noon and midnight), cloud and surface IR temperatures and UV reflectivities, detection of cloud with different retrieval algorithms (infrared and bispectral), distributions of some specific cloud types (cirrus, deep convective, and warm-low), and the spatial and temporal variation of all of these parameters.

In this study, the results of analysis of the first data year, April 1979–March 1980, have been presented. The following has been concluded:

1) Inclusion of an ultraviolet reflectance algorithm with an IR algorithm results in the identification of greater low cloud amounts (10%–40%) than found by the IR-only algorithm for the west coasts of North and South America, southwestern Africa, and the Arctic Ocean area for July 1979. In January, the bispectral algorithm also detected more cloud than the IR-only algorithm over the land areas of North America and Eurasia and the high latitude southern oceans.

2) Based only on IR algorithm results, the midnight cloud amounts are greater than noon cloud amounts, in the zonal mean, for nearly all latitudes in both July and January. Over oceans, the areas which show the largest increases in cloudiness at midnight are areas prevalent with low and midlevel cloud, often stratus or stratocumulus, which commonly exhibit thinning and fragmentation due to solar heating at midday. Over land, the areas with the largest increase in cloud at midnight relative to noon are regions of mid and high level cloud, where late afternoon/evening deep convective activity occurs. The largest increases at midnight are in the African continent between about 5°–20°N, where cloud amount is typically 20%–40% greater at midnight in July.

3) In July, low (<2 km altitude) cloud amounts are less than 10% for the majority of land regions, since surface moisture is relatively low, while most ocean areas are covered by 10%–30% low cloud. The exception is the ITCZ region where recorded low cloud amounts are less than 10%, probably because many low clouds were obscured from satellite view by large amounts of mid and high level clouds. In January, excluding 60°–90°S, the maximum global low cloud amount (30%–50%) occurs in the Mongolian region, where strong high pressure limits the vertical development of clouds. Without the unique “warm cloud” logic of the Nimbus-7 IR algorithm, much of this cloud would go undetected.

4) Amounts of mid (altitude from 2–7 km in tropics to 2–4 km near the poles) level cloud are maximum in the ITCZ, monsoon regions, and Antarctic ocean waters from 50°–70°S. They are at a minimum over deserts and oceanic subtropical high pressure regions. Midlevel cloud amounts from Nimbus-7 agree well with Air Force 3DN amounts (Henderson-Sellers 1986) except for stratocumulus regions where the 3DN classification is low cloud.

5) High (altitude above upper midcloud boundary) cloud amounts in July 1979 are at a maximum in the Indian and Asian monsoon regions and the ITCZ, while in January 1980, the ITCZ is less well defined with a large gap in the east Pacific. There is good agreement in the geographical distribution of high clouds between the Barton (1983) and Nimbus-7 climatologies. However, the magnitude of Barton’s high cloud amounts are about 10% greater. This may be due to the Nimbus-7 algorithm misidentifying thin cirrus (emissivity <1) as midlevel cloud, and because Barton defines the high cloud boundary at 6 km in the tropics while it is 7 km for Nimbus-7.

6) Cirrus cloud detected by the Nimbus-7 algorithm for January 1980 is at a global maximum in the Indonesian region southward towards Australia (15%–25%), with amounts of 5%–10% occurring in other regions of the ITCZ. In July 1979 the Nimbus-7 cirrus estimates are a maximum immediately to the south of India, across Indonesia, and immediately west of Central America. For both seasons, the frequency of occurrence of cirrus observed by ships (Hahn et al. 1982) is also a maximum over these regions. However, there are regions in the North Pacific and North Atlantic where ship-observed frequency of occurrence of cirrus is high (40%–45%) and Nimbus-7 cirrus cloud fraction is low (<5%). These differences are probably due to the combination of the inability of the Nimbus-7 cirrus algorithm to detect cirrus in multilayer cloud situations, while ship observers can, and the difficulties in comparing cloud fraction with frequency of occurrence.

7) Deep convective cloud, which is identified by the Nimbus-7 bispectral algorithm, also has a local maximum (5%–15%) in the area of the southeast Asian/Indonesian and Indian Ocean ITCZ region in January

1980. These are also regions of maximum frequency of occurrence of cumulonimbus (Cb) cloud observed by ships. However, there are several middle to high latitude areas over ocean where the Nimbus-7 deep convective amounts are relatively high (5%–15%) and the frequency of occurrence of Cb by ships is very low. These areas correspond to regions where the probability of simultaneous occurrence of high cirrus and low stratus or nimbostratus is very high according to ship reports (Hahn et al. 1982). Thus, these multilayer clouds perhaps are being misidentified as deep convective cloud by the Nimbus-7 algorithm. Also, errors in sea/ice identification could lead to a false classification of deep convective by the bispectral algorithm.

8) The hemispheric and global averages of scene radiance for January 1980 and July 1979 suggest: (i) each hemisphere is radiatively colder in its winter season and warmer in its summer season, (ii) the globe is radiatively warmer in July than in January, (iii) both hemispheres (and hence the globe) are radiatively brighter in January than in July in the UV part of the solar spectrum.

9) The hemispheric and global averages of clear-sky and cloud radiative temperature for the two months studied indicate 1) the clear-sky radiative temperature of the Earth is greatest in July and least in January, with the respective winter hemisphere having lower temperatures than the summer hemisphere, consistent with the scene radiance analysis; 2) this is also observed for the low, mid, and high cloud radiative temperatures; 3) the extremes in hemispherically averaged radiative temperature occur in July, where the Northern Hemisphere clear-sky temperature is 295 K and the Southern Hemisphere high cloud temperature is 232 K.

10) Analysis of the differences between local noon and midnight scene radiative temperatures for four different cloud amount categories, and the frequency of occurrence of these categories, over land and ocean for December through February in the Southern Hemisphere tropics indicated that: (i) land and ocean have distinctly different cloud amount/radiance characteristics; (ii) over land, noon radiances are larger than midnight radiances for all clear/cloud categories, and the frequency of occurrence of the four categories monotonically increases with increasing cloud amount, although the increase is less uniform for noon than for midnight; (iii) over ocean, contrary to the land scenes, mostly cloudy and overcast regions have higher (warmer) scene radiances at midnight than at noon, and partly cloudy is the most frequently occurring cloud category both at noon and at midnight, having a higher frequency of occurrence at noon with the bispectral algorithm result than with either the infrared-only noon or midnight results. These differences between land and ocean cloud characteristics are most probably related to differences in the diurnal change in surface temperature of ocean and land regions.

11) Zonal means of total cloud from the Nimbus-

7 algorithm were compared with the multilayer cloud climatology of London (1957), based on surface observations; Berlyand and Strokina (1980a,b), based mainly on surface observations but including some satellite observations; and the Air Force 3DN for 1979 (Hughes and Henderson-Sellers 1985) based on satellite and other data sources. In addition, a comparison was made with preliminary ISCCP algorithm (Rossow et al. 1985) noon cloud products for July 1983. Excluding the polar regions, the Nimbus-7 is in good agreement with the climatologies in the location of the latitudes of minimum and maximum cloudiness. However, it is notable that the difference between the ITCZ maximum cloud amount and the subtropical minima cloud amount are much greater for the Nimbus-7 than for the other climatologies, with the 3DN estimates in closest agreement with the Nimbus-7. The differences between the Nimbus-7 and the London and Berlyand and Strokina climatologies may be due to the effect of time averaging in the multiyear data sets and to the lack of a high resolution surface observation network in the tropics. However, the marked differences between the Nimbus-7 and ISCCP for July 1983 must be laid to significant differences in the cloud estimation algorithms. A further study of these algorithm differences and their effects is needed.

12) Detection of clouds in polar regions is very difficult and the four climatology data sets examined show large differences and high variability for both the north and south polar regions.

13) Hemispheric averages were computed and all climatologies, other than London's (Northern Hemisphere only), agree that, except for July, the Southern Hemisphere cloudiness is greater than the Northern Hemisphere by as much as 10%, and the maximum hemispheric cloud amount occurs in the respective summer and the minimum in the respective winter seasons.

14) Globally and seasonally averaged cloud amount for the first data year from Nimbus-7 is 51% (49% w/o TOMS) at local noon and 56% at local midnight. London's value is closest to the local noon estimate while the 3DN value is closest to the local midnight value. The Berlyand and Strokina value is greatest of all at 60%. However, from the preliminary July 1983 ISCCP data studied (Fig. 15), it appears that the ISCCP cloud estimates will average over 60%.

15) A comparison between the cloud amounts at three height categories from London (1957) and Nimbus-7 has shown that for nearly all latitude zones in both July and January, the low cloud is the predominant type for London's climatology, while mid cloud predominates in the Nimbus-7 data set. This discrepancy results from differences in the definition of cloud altitude between Nimbus-7 and surface observations. Surface observers define cloud altitude principally by base height while in the Nimbus-7 algorithm, the height is determined by cloud top IR radiance. Also, for the

case of multilayer clouds, the surface observer will report the base height of the lowest layer while the satellite will measure radiances from the top of the highest layer. Therefore, only for a relatively thin, single layer, opaque cloud will the two observations yield the same cloud height.

Analysis of the first year data set of the Nimbus-7 global cloud climatology has shown that there is a wealth of information about cloud amounts, cloud types, cloud and scene radiances, day-night cloud differences, and the seasonal variation of these parameters. This data set provides insight into the results of various threshold cloud detection algorithms and a fuller understanding of global cloud distributions and properties in comparison with other cloud climatologies.

Acknowledgments. The authors would like to thank Dr. E. J. Hurley of NASA/GSFC for continuous encouragement, and Kathy Leo, Jennifer Forman, and Cherrie Johnson of ST Systems Corporation for help with the preliminary manuscript and Brenda Vallette of Research and Data Systems Corporation for preparation of the final manuscript. We are appreciative of Mr. R. Ryan of NOAA/NESDIS who drafted some of the figures. The authors are also indebted to Dr. W. Rossow, of NASA/GISS, for valuable discussions about the results from the ISCCP intercomparison, and to Professor R. Cess, of SUNY at Stony Brook, for permitting use of a figure illustrating ISCCP/Nimbus-7 differences.

REFERENCES

- Barton, I. J., 1983: Upper level cloud climatology from a orbiting satellite. *J. Atmos. Sci.*, **40**, 435–447.
- Berlyand, T. G., and L. A. Strokina, 1980a: Zonal cloud distribution on the Earth. *Meteor. Gidrol.*, **3**, 15–23.
- , and —, 1980b: Global distribution of total cloud amount. *Gidrometeoizdat*, Leningrad, 18 pp.
- Coakley, J. A., 1987: A dynamic threshold method for obtaining cloud cover from satellite imagery data. *J. Geophys. Res.*, **92**(D4), 3985–3990.
- , and F. P. Bretherton, 1982: Cloud cover from high-resolution scanner data: detecting and allowing for partially filled fields-of-view. *J. Geophys. Res.*, **87**(C7), 4917–4932.
- Cox, S. K., 1969: Radiation models of mid-Latitude synoptic Features. *Mon. Wea. Rev.*, **97**, 637–651.
- Curry, J. A., and G. F. Herman, 1985: Relationships between large-scale heat and moisture budgets and the occurrence of Arctic stratus clouds. *Mon. Wea. Rev.*, **113**, 1441–1457.
- d'Almeida, G. A., 1987: On the variability of desert aerosol radiative characteristics. *J. Geophys. Res.*, **92**, 3017–3026.
- Duvel, J. P., and R. S. Kandel, 1985: Regional-scale diurnal variations of outgoing infrared radiation observed by METEOSAT. *J. Climate Appl. Meteor.*, **24**, 335–349.
- Eck, T. F., P. K. Bhartia, P. H. Hwang and L. L. Stowe, 1987: Reflectivity of Earth's surface and clouds in ultraviolet from satellite observations. *J. Geophys. Res.*, **92**(D4), 4287–4296.
- Fye, F. K., 1978: The AFGWC Automated Cloud Analysis Model. HQ AFGWC, TM-78 002, Air Force Global Weather Central, Nebraska, 97 pp.
- Gordon, C. T., 1984: Personal Communication of London's Zonal Cloud Data Used at NOAA/GFDL.
- Gray, W. M., and R. W. Jacobson, 1977: Diurnal variation of deep cumulus convection. *Mon. Wea. Rev.*, **105**, 1171–1188.
- Hahn, C. J., S. G. Warren, J. London, R. M. Chervin and R. Jenne, 1982: Atlas of simultaneous occurrence of different cloud types over the ocean. NCAR Tech. Note TN-201 + STR, 212 pp. [NTIS PB83-152074.]
- , —, —, and —, 1984: Atlas of simultaneous occurrence of different cloud types over land. NCAR Tech. Note TN-241 + STR, 214 pp.
- Hansen, J., G. Russell, D. Rind, P. Stone, A. Lacis, L. Travis, S. Lebedeff and R. Ruedy, 1983: Efficient three-dimensional global models for climate studies: Models I and II. *Mon. Wea. Rev.*, **111**, 609–662.
- Hanson, H. P., and P. L. Gruber, 1982: Effect of marine stratocumulus clouds on the ocean surface heat budget. *J. Atmos. Sci.*, **39**, 897–907.
- Hartmann, D. L., and E. E. Recker, 1986: Diurnal variation of outgoing longwave radiation in the tropics. *J. Climate Appl. Meteor.*, **25**, 800–812.
- Henderson-Sellers, A., 1986: Layer cloud amounts for January and July 1979 from 3D-Nephanalysis. *J. Climate Appl. Meteor.*, **25**, 118–132.
- , and N. A. Hughes, 1985: 1979 3D-nephanalysis global total cloud amount climatology. *Bull. Amer. Meteor. Soc.*, **66**, 626–627.
- Herman, G. F., and R. M. Goody, 1976: Formation and persistence of summertime Arctic stratus clouds. *J. Atmos. Sci.*, **33**, 1537–1553.
- Hobbs, P. V., 1981: Scales involved in the formation and organization of clouds and precipitation. *Clouds: Their Formation, Optical Properties, and Effect*, P. V. Hobbs and A. Deepak, Ed., Academic Press, 497 pp.
- Hughes, N. A., 1984: Global cloud climatologies: A historical review. *J. Climate Appl. Meteor.*, **23**(5), 724–751.
- , and A. Henderson-Sellers, 1985: Global 3D-Nephanalysis of total cloud amount: Climatology for 1979. *J. Climate Appl. Meteor.*, **24**(7), 669–686.
- Hwang, P. H., Ed., 1982: Nimbus-7 Temperature Humidity Infrared Radiometer (THIR) data user's guide. NASA/Goddard Space Flight Center, Greenbelt, MD 20771, 52 pp.
- , H. Y. M. Yeh, D. MacMillan and C. Long, 1986: Validation of Nimbus-7 cloud and SMMR data. Preprints, *AMS Second Conference Satellite Meteorology/Remote Sensing*, Williamsburg, VA, Amer. Meteor. Soc., 405–408.
- , L. L. Stowe, H. Y. M. Yeh, H. L. Kyle and Nimbus-7 Cloud Data Processing Team, 1988: The Nimbus-7 global cloud climatology. *Bull. Amer. Meteor. Soc.*, **69**, 743–752.
- Jacobowitz, H., H. V. Soule, H. L. Kyle, F. B. House and Nimbus-7 ERB Experiment Team, 1984: The Earth Radiation Budget (ERB) Experiment: An Overview. *J. Geophys. Res.*, **89**(D4), 5021–5038.
- Jenne, R. L., H. L. Crutcher, H. VanLoon and J. J. Taljaard, 1974: A selected climatology of the southern hemisphere: Computer methods and data availability. NCAR Tech. Note NCAR-TN/STR-92, National Center for Atmospheric Research, Boulder, CO, 95 pp.
- Kyle, H. L., P. E. Ardanuy and E. J. Hurley, 1985: "The Status of the Nimbus-7 ERB Earth Radiation Budget Data Set." *Bull. Amer. Meteor. Soc.*, **66**, 1378–1388.
- Liou, K. N., and Q. Zheng, 1984: Numerical experiment of the interactions of radiation, cloud and dynamic processes in a general circulation model. *J. Atmos. Sci.*, **41**, 1513–1535.
- London, J., 1957: A study of the atmospheric heat balance. Final Report, Contract AF 19(122)-165 (AF CFC-TR-57-287), New York Univ., 99 pp.
- Meleshko, V. P., and R. T. Wetherald, 1981: The effect of a geographical cloud distribution on climate: A numerical experiment with an atmospheric general circulation model. *J. Geophys. Res.*, **86**, 11 995–12 014.
- Minnis, P., and E. F. Harrison, 1984: Diurnal variability of regional cloud and clear-sky radiative parameters derived from GOES data. Part II: November 1978 cloud distributions. *J. Climate Appl. Meteor.*, **23**, 1012–1031.
- Nakamura, N., and A. H. Oort, 1988: Atmospheric heat budgets of the polar regions. *J. Geophys. Res.*, **93**(D8), 9510–9524.

- Ohring, G., and P. Clapp, 1980: The effect of changes in cloud amount on the net radiation at the top of the atmosphere. *J. Atmos. Sci.*, **37**(2), 447–454.
- , T. S. Chen, L. L. Stowe, B. Morse, P. P. Pellegrino and C. S. Long, 1986: Sensitivity of the Earth radiation budget to changes in cloudiness as determined from Nimbus-7 satellite data. Preprints, *AMS Sixth Conference on Atmospheric Radiation*, Williamsburg, VA, Amer. Meteor. Soc., 266–267.
- Rossow, W. B., F. Moshier, E. Kinsella, A. Arking, M. Desbois, E. Harrison, P. Minnis, E. Ruprecht, G. Seze, C. Simmer and E. Smith, 1985: ISCCP cloud algorithm intercomparison. *J. Climate Appl. Meteor.*, **24**, 877–903.
- Schneider, S. H., 1972: Cloudiness as a global climatic feedback mechanism: The effects on the radiation balance and surface temperature of variations in cloudiness. *J. Atmos. Sci.*, 1413–1422.
- Schwerdfeger, W., 1984: *Weather and Climate of the Antarctic*. Elsevier, 261 pp.
- Seze, G., and W. B. Rossow, 1989: Effects of satellite data resolution on measuring the space/time variations of surfaces and clouds. (submitted to *J. Climate*).
- , F. Drake, M. Desbois and A. Henderson-Sellers, 1986: Total and low cloud amount over France and Southern Britain in the summer of 1983: Comparison of surface-observed and satellite-retrieved values. *Int. J. Remote Sensing*, **7**, 1031–1050.
- Smith, G. L., R. N. Green, E. Raschke, L. M. Avis, J. T. Settles, B. A. Wielicki and R. Davies, 1986: Inversion methods for satellite studies of the Earth's radiation budget; development of algorithms for the ERBE mission. *Rev. Geophys.*, **24**, 407–421.
- Stowe, L. L., 1984: Evaluation of Nimbus-7 THIR/CLE and Air Force Three-Dimensional Nephelometer Estimates of Cloud Amount. *J. Geophys. Res.*, **89**(D4), 5370–5380.
- , P. Pellegrino, P. H. Hwang, P. K. Bhartia, T. F. Eck, C. G. Wellemeyer, S. M. Read and C. S. Long, 1984: Validation of Nimbus-7 Cloud Products. *Proc. International Radiation Symposium*, Perugia, Italy, A. Deepak, 228–231.
- , —, —, —, —, C. S. Long, C. G. Wellemeyer and H. Y. M. Yeh, 1986: Spatial and temporal characteristics of global cloud cover as observed from the Nimbus-7 satellite. Preprints, *AMS Sixth Conference on Atmospheric Radiation*, Williamsburg, VA, Amer. Meteor. Soc., 99–102.
- , C. G. Wellemeyer, T. F. Eck, H. Y. M. Yeh and Nimbus-7 Cloud Data Processing Team, 1988: Nimbus-7 global cloud climatology. Part I: Algorithm and validation. *J. Climate*, **1**, 445–470.
- Vowinkel, E., and S. Orvig, 1970: The climate of the north polar basin. *Climates of Polar Regions World Survey of Climatology*, Vol. 14, S. Orvig, Ed., Elsevier, 370 pp.
- Warren, S. G., 1982: Optical properties of snow. *Rev. Geophys. Space Phys.*, **20**, 67–89.
- , and S. L. Thompson, 1983: The climatological minimum in tropical outgoing infrared radiation: contribution of humidity and clouds. *J. Roy. Meteor. Soc.*, **109**, 169–185.
- , C. J. Hahn and J. London, 1985: Simultaneous occurrence of different cloud types. *J. Climate Appl. Meteor.*, **24**, 658–667.
- , C. J. Hahn, J. London, R. M. Chervin and R. L. Jenne, 1986: Global distribution of total cloud-cover and cloud type amounts over land, NCAR Tech. Note TN/STR-273, National Center for Atmospheric Research, 468 pp.
- Yeh, H. Y. M., P. H. Hwang, T. F. Eck, C. G. Wellemeyer, P. K. Bhartia, L. L. Stowe and C. S. Long, 1986: Intercomparison between Nimbus-7 cirrus cloud data and ERB measurements. Preprints, *AMS Sixth Conference on Atmospheric Radiation*, Williamsburg, Amer. Meteor. Soc., 276–279.